A Resource for the State of Florida

HURRICANE LOSS REDUCTION
FOR
HOUSING IN FLORIDA:

PERFORMANCE OF TILE ROOFS UNDER HURRICANE IMPACT – PHASE 2

A Research Project Funded by
The State of Florida Division of Emergency Management
Through Contract # 06RC-A%-13-00-05-261

Prepared by:
Amir Mirmiran, Ton-Lo Wang, Caesar Abishdid,
Peng Huang, Diego L. Jiménez, and Chadi Younes
Department of Civil and Environmental Engineering
Florida International University

In Partnership with:
The International Hurricane Research Center
Florida International University

August 2007

TABLE OF CONTENTS

LIST OF FIGURES

LIST OF TABLES

EXECUTIVE SUMMARY

In the past few years, the State of Florida has suffered the impact of an unprecedented number of hurricanes, resulting in an immense regional and local economic impact. The damage from some of the rather smaller hurricanes has challenged the building codes in South Florida as they relate to roof covering. While most homes suffered little structural damage, many experienced roof covering failures, and especially lost a large number of roof tiles.

The main issues at hand are; (a) whether there is a significant difference in performance of clay and concrete tiles under different attachment methods and, if so, why, (b) whether the current building codes provide adequate and reasonable measures for proper performance of tile roofs, and (c) what, if any, change is necessary to improve the way tile roofs are installed.

A detailed experimental and analytical study was carried out for, field and ridge tiles of clay or concrete with adhesive-set or mortar-set. The experimental study entailed testing individual tiles as well as full-scale sections of roofs with both field and ridge tiles. The strongest system appeared to be concrete tiles with mortar under both, mechanical uplift and simulated wind load. While concrete tiles bond to mortar much better than clay tiles, clay tiles adhere better to the foam. Concrete tiles also perform better than clay tiles when impacted by a projectile. The present study does not support recent efforts by the industry to completely ban the use of mortar for all attachments of hip and ridge tiles. However, it is suggested that any such ban on mortar be limited to clay tiles only.

Roof tile failures seem to initiate at the eave on the windward side of the roof, after which a progressive domino failure pattern was observed. Setting pattern of the tiles may also help develop a better inter-locking arrangement for the entire roof. Workmanship was found to be the main contributing factor to roof tile failures, as confirmed by tests and analysis.

Specific recommendations arising from this detailed study on the performance of tile roofs under hurricane impact are twofold:

- Special attention should be paid to the attachment of eave tiles, as they are the most vulnerable to failure, and as their failure can result in loss of large section of the roof.
- Inspection procedures should be put in place to ensure roofing contractors closely follow the standard techniques of roof tile installation, as the poor workmanship was found to be the main contributing factor to roof failures.

Performance of Tile Roofs under Hurricane Impact – Phase 2

Amir Mirmiran, Ton-Lo Wang, Caesar Abishdid
Peng Huang, Diego L. Jimenez, and Chadi Younes

1.0 Introduction

1.1 Statement of the Problem

Widespread damage to tile roofs across South Florida over the last few years, especially for the Category 1 Hurricane Wilma in October 2005, has raised concerns regarding tile roof construction practices in Florida, and in particular, questions as to whether there are any differences between the performance of clay and concrete tiles.

Funded by the Florida Department of Community Affairs (FDCA) through the International Hurricane Research Center (IHRC), Phase 1 of this research set out to determine (a) whether there is a significant difference in performance of clay and concrete tiles and, if so, why, (b) whether the current building codes provide adequate and reasonable measures for proper performance of tile roofs, and (c) what, if any, change is necessary to improve the way tile roofs are installed.

A detailed experimental and analytical study was carried out for ridge clay and concrete tiles with (a) adhesive-set, (b) mortar-set, and (c) mechanical attachments. The strongest system appeared to be concrete tiles with mortar. While concrete tiles bonded to mortar much better than clay tiles, clay tiles adhered better to the foam. Concrete tiles also performed better than clay tiles, when mechanical fasteners were used with an embedment length of at least 1". As a result, the study did not support recent efforts by the industry to completely ban the use of mortar for all attachments of hip and ridge tiles. However, it suggested that any such ban on mortar be limited to clay tiles only.

It is important to note that the findings of Phase 1 were preliminary, as it was limited to single ridge tiles. It was therefore, found necessary to extend the study to include testing of a larger section of the roof with field tiles made of clay or concrete. Also, cyclic and dynamic loading of tiles can better simulate the effects of hurricane wind forces. This may also be achieved through large-scale wall-of-wind tests of clay and concrete tile roofs.

1.2 Research Objectives

The following research objectives were established to address the above stated problems:

- Assess uplift resistance of clay and concrete tiles for a section of the roof with field tiles and hip or ridge tiles, and with different attachment systems;
- Assess the effect of cyclic loading and load reversal on the uplift resistance of clay and concrete tiles;

- Compare the performance of clay and concrete tiles under projectile impact; and
- Evaluate the performance of a large section of roof with clay or concrete tiles under the impact of simulated wind loads.

1.3 Research Methodology

1.3.1 Survey of Literature and Practice

An extensive survey was carried out in Phase 1 to identify the current practice and building code requirements for the various roof covering attachment systems. The review section also covered investigations by the roof tile industry and different government agencies on the performance of tile roofs under the impact of recent hurricanes. This study looked at some of the more recent reports published by local and federal agencies that outlined the damage incurred by different types of tile roof systems under hurricane winds. The review section also covers the limited literature available on the different methods of wind load testing of tile roofs to ensure that the proposed experimental work fits well with the standard practices of the industry.

1.3.2 Performance Assessment of Tile Roofs with Modeling and Full-Scale Testing

Based on the literature investigation, several experimental models were built to test all permutations of the two types of roof tiles and the two types of attachments. Clay and concrete ridge and field tiles with mortar-set and adhesive-set (foam) were tested. Some tests involved full-scale roof sections, while others consisted of single tile tests. In all, three types of tests were carried out, as follows:

- Mechanical Uplift Testing: Specimens were built with a small section of the roof including field and hip/ridge tiles made of clay or concrete tiles and different attachments systems (mortar or foam). The specimens were subjected to two types of loading; (a) monotonic uplift load, and (b) cyclic pseudo-static uplift load. The loads were applied at critical location(s).
- Impact testing: Lumber projectiles fired from an air canon, as well as drop-ball tests were performed on full-scale roof section and single tiles.
- Wind Load Testing: Full-scale roof sections were built on a scaled house structure, and were subjected to distributed wind pressure simulating Category 1 or 2 hurricanes. Tests were conducted using the Wall of Wind equipment.

Test data was then fed into a finite element model (FEM) of a roof section that included the tiles, the backing materials, and the roof truss. The FEM provided an accurate tool for the analysis of the entire roof system.

1.3.3 Guidelines and Recommendations

Guidelines and recommendations are presented in order to improve resistance of tile roofs in Florida. These recommendations affect current practices as well as current building code requirements. They also include suggestions for future research.

1.4 Organization of the Report

This report is divided into seven sections: (1) Introduction, (2) Literature Review, (3) Mechanical Uplift Testing, (4) Impact Testing, (5) Wall of Wind (WoW) Testing, (6) Finite Element Modeling, and (7) Conclusions. Section 1, this section, presents the problem statement, and objectives and methodology. Section 2 presents a review of roof tile attachment methods, post-hurricane assessment reports, and codes and regulations. Section 3 is devoted to the test results of concrete and clay tiles for their physical properties and monotonic and cyclic uplift resistance. Section 4 shows the results from the various impact tests performed on a variety of roof tile systems. Section 5 presents the results of the WoW testing for full-scale roof sections under different wind speeds and angles of exposure. Section 6 illustrates the results of a finite element analysis of a roof section subject to a hurricane wind forces. Conclusions and recommendations are presented in Section 7.

2.0 Literature Review

Literature was presented in Phase 1 report identifying the current practice and building code requirements for the various roof covering attachment systems. The review section also covered investigations by the roof tile industry and different government agencies on the performance of tile roofs under the impact of recent hurricanes. This study reviewed some of the more recent reports published by local and federal agencies that outlined the damage incurred by different types of tile roof systems under hurricane winds. This review section briefly summarizes the findings of the literature surveyed in Phase 1, as well as the literature available on full-scale wind testing of the performance of tile roof sections.

Phase 1 report presented a detailed review of the three attachment methods for roof tiles used in Florida: mechanical, adhesive-set and mortar-set. Mechanically attached systems can use either nails or screw fasteners. One screw or nail is used to attach each tile in addition to an adhesive agent at the tile overlaps. Mortar consists of cement conforming to ASTM C 91 Type M, sands conforming to ASTM C 144, and other lightweight aggregates meeting ASTM C 332 requirements. Adhesive-set is a fairly new system developed in response to a widespread failure of tiles attached using the mortar-set systems under the impact of Hurricane Andrew.

A detailed review of the codes and regulations governing the material, testing, and construction of tile roofs in Florida was also covered in Phase 1 report. Building construction in Florida is regulated by the Florida Building Code (FBC). According to the FBC, all building construction in Miami-Dade and Broward counties is governed by Zone 2, High Velocity Hurricane Zone (HVHZ). The installation of clay and concrete tiles is regulated by Section 1507.3 of the FBC and shall comply with recommendations of the Florida Roofing, Sheet Metal and Air Conditioning Contractors Association (FRSA) and the Tile Roofing Institute (TRI). Testing procedures in the High Velocity Hurricane Zones are provided in Section 1523 of the FBC. This section defines minimum testing requirements for roofing components, and requires that all roofing products be tested for their physical properties, water infiltration, and uplift resistance. Miami-Dade County further requires that all building products and components being considered for installation within its jurisdiction be approved by the county's Product Control Division prior to their use

Phase 1 report also provided an overview of some of the post-hurricane assessment team reports for storms that impacted Florida in 2004 and 2005. The following summarizes the assessments that were consistently made by different teams deployed by the tile industry to the impacted areas:

- Tile roofs attached using mortar-set systems sustained more damage than those using adhesive-set or mechanically fastened systems.

- Improper installation was found to be a critical contributing cause to the damages, especially in adhesive-set systems, where either the size of the foam paddy was

insufficient or the foam was not allowed to adequately cure before placing the tiles.

- Widespread problems were noted with the hip and ridge tiles, especially for those using only mortar-set, in which most often an insufficient amount of mortar was placed.

- Workmanship defects were found in the installations, for example, mortar layer was thin and sometimes did not come in contact with the tile, or often inadequate adhesives were applied under the tiles, or in a significant variance from the manufacturers' guidelines, adhesive was applied in straight lines.

Phase 1 report also presented the conclusions of the FEMA deployed Mitigation Assessment Teams (MAT). These MAT reports concluded that current static test methods used to evaluate tile performance may over-estimate the actual resistance of tiles, as they neglect the dynamic load impact of a hurricane. In addition to other recommendations concerning the installation procedures, inspections, product testing, and training and certification programs for tile manufacturers were discussed.

Phase 1 report also outlined the changes to the FBC recommended by a coordination group tasked with the identification and evaluation of research projects regarding building failures in the 2004 hurricane season. Changes in tile attachment methods, material approval, and testing requirements were among the most highly recommended ones. Widespread hurricane damage to hip and ridge tiles resulted in the development of an intensive set of guidelines for hip and ridge tile installation, which was adopted into the FBC and incorporated into the latest edition of the TRI/FRSA *Concrete and Clay Roof Tile Installation Manual* for Florida.

Despite the MAT recommendations and the widespread agreement on the lack of accuracy of the results of static tests, very little information is available on dynamic load testing of full-scale tile roof sections. No research has yet been done, or at least documented, on full-scale tile roofs using dynamic wind loading. This is where the significance of the present study lies. This work represents the first in-depth look at the behavior and performance of tile roofs under hurricane winds using full-scale dynamic testing.

3.0 Mechanical Uplift Testing

Mechanical loading tests were conducted on concrete and clay tiles to obtain their uplift resistance when attached with adhesive or mortar sets. Monotonic and cyclic load tests were performed on ridge tiles, while field tiles were only evaluated under monotonic loading. All tiles were installed following the procedures outlined in the *Concrete and Clay Roof Tile Installation Manual*.

3.1 Uplift Resistance of Ridge Tiles with Adhesive-Set

These tests were conducted in accordance with ASTM C 1568. A ¼" diameter hole was drilled at the center of each tile, and a ¼" steel bolt was fastened to the tile to apply an upward force. A 3/8" washer was placed under each tile to increase the contact area of the applied force and to avoid premature failure due to stress concentration. The tiles were then attached with Polypro AH 160 roof tile adhesive to a 2"x 6" ridge board that was mechanically fastened to the roof deck, as shown in Figure 3.1. The average weight of the foam paddies was approximately 30 grams per tile. Figure 3.2 shows the typical foam paddy size. The framing system consisted of a ½" plywood decking mounted on 2"x 4" rafters spaced at 24" on center.

Unlike Phase 1, in which only single tile specimens were evaluated, the present study evaluates multiple ridge tile assemblies representative a typical ridge section of the roof. Three overlapping tiles were used for each specimen, as shown in Figure 3.3. This overlap better represents field conditions, whereby the neighboring tiles affect the uplift on the center tile. The average overlap between tiles was approximately 2 in. Six specimens were set up for each attachment system; three were tested by pulling all three ridge tiles simultaneously, while the other three were tested by pulling only the center tile.

In addition to obtaining the uplift resistance of different attachment systems, the mode of failure for each of the four systems was also determined. Four possible failure modes were identified for the adhesive-set systems: (1) bonding failure at the interface between the tile and the foam, (2) bonding failure at the interface between the ridge board and the foam, (3) failure within the foam paddy itself, and (4) bearing failure of the tile at the point of load application. It should be noted that under hurricane winds, the uplift pressure is distributed over the entire exposed area of the tile, and therefore, tiles are not subject to high stress concentration. It was therefore decided to distribute the applied load and avoid bearing failure of the tile at the point of load application as much as possible.

3.1.1 Three Tile Assembly Subjected to Center-Point Loading

Three (3) clay and three (3) concrete ridge tile specimens were set up with adhesive-set, kept inside the lab at room temperature, and tested 3 days later by pulling only the center tile.

Tables 3.1 Table 3.2 and 3.2 list test results for clay and concrete tiles with adhesive-set, respectively. The failure load was taken as the load required to cause additional deflection without any further uplift resistance.

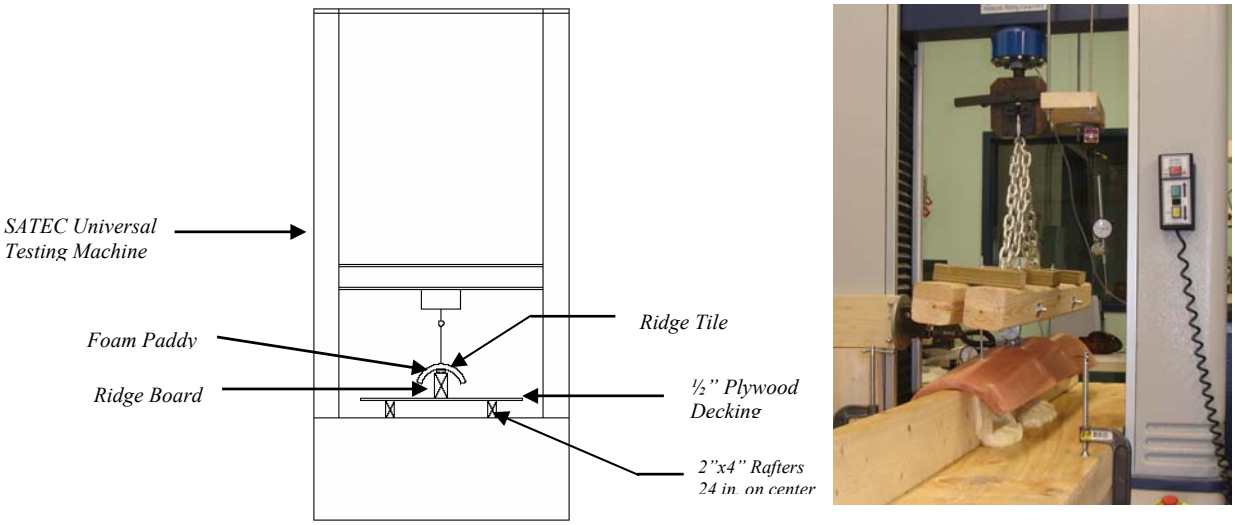

Figure 3.1: Testing Apparatus and Set-Up for Roof Tiles with Adhesive-Set

Figure 3.2: Typical Foam Installation

Figure 3.3: Three- Tile Specimens

Table 3.1: Test Results of Clay Tiles with Adhesive–Set

Specimen No.	Uplift Resistance (lbs)	Failure Mode
1	585	Load Point
2	595	Debonding of Foam from Ridge Board
3	600	Debonding of Foam from Ridge Board
Average	593	

Table 3.2: Test Results of Concrete Tiles with Adhesive-Set

Specimen No.	Uplift Resistance (lbs)	Failure Mode
1	310	Debonding of Ridge Tile from Foam
2	280	Debonding of Ridge Tile from Foam
3	283	Debonding of Ridge Tile from Foam
Average	291	

As was also the case in Phase I, clay tiles exhibited bonding failure at the interface between the adhesive foam and the ridge board, while concrete tiles exhibited bonding failure at the interface between the tile and the adhesive foam. The average uplift resistance of concrete tiles was found to be 291 lbs. The average uplift resistance of clay tiles was 593 lbs, more than twice that of concrete tiles.

Figures 3.4 and 3.5 show typical failure modes of clay and concrete tiles, respectively. As seen in the figures, little or no foam remained bonded to concrete tiles after failure, while most of the foam remained bonded to clay tiles.

Figure 3.4: Typical Failure Surface of Adhesive-Set with Clay Tile

Figure 3.5: Typical Failure Surface of Adhesive-Set with Concrete Tile

These results were very consistent with those obtained in Phase 1. The average uplift resistance obtained in Phase I for clay and concrete tiles attached with adhesive-set were 547 lbs and 305 lbs respectively. These results further confirm that adhesive-set adheres better to clay tiles than to concrete tiles.

3.1.2 Three Tile Assembly Subjected to Three-Point Loading

Three (3) clay and three (3) concrete ridge tile specimens were set up with adhesive-set, kept inside a lab at room temperature, and tested 3 days later by pulling on all three of the tiles simultaneously.

Tables 3.3 and 3.4 summarize the test results for adhesive-set with clay and concrete tiles, respectively. The failure load was taken to be the load required to cause additional deflection without any further uplift resistance.

Table 3.3: Test Results of Clay Tiles with Adhesive–Set

Specimen No.	Uplift Resistance (lbs)	Failure Mode
1	412	Debonding of Foam with Ridge Board
2	479	Debonding of Foam with Ridge Board
3	300	Debonding of Foam with Ridge Board
Average	397	

Table 3.4: Test Results of Concrete Tiles with Adhesive-Set

Specimen No.	Uplift Resistance (lbs)	Failure Mode
1	314	Debonding of Ridge Tile with Foam
2	295	Debonding of Ridge Tile with Foam
3	241	Debonding of Ridge Tile with Foam
Average	283	

Figures 3.6 and 3.7 show typical failure modes of adhesive-set with clay and concrete tiles, respectively. Concrete tiles exhibited bonding failure at the interface between the tile and the adhesive foam, while clay tiles exhibited bonding failure between the foam and the ridge board. The average uplift resistance for concrete tiles was found to be 283 lbs, while it was 397 lbs for clay tiles. The higher uplift resistance and the exhibited failure mode constitute irrefutable evidence that the foam adheres better to clay tiles than it does to concrete tiles.

Figure 3.6: Typical Failure Surface of Adhesive-Set with Clay Tile

Figure 3.7: Typical Failure Surface of Adhesive-Set with Concrete Tile

3.2 Uplift Resistance of Ridge Tiles with Mortar-Set

These tests were performed in accordance with the Testing Application Standards (TAS). The installation was similar to the tiles with adhesive-set, except for the use of 1" diameter washer. Figure 3.8 shows the test set up for the mortar–set attachment. The ridge tiles were attached with mortar-set to the field tiles that had been mechanically fastened to a ½" plywood decking. The deck was then mounted on 2"x 6" rafters spaced at 24" on center. This set-up represents the actual field conditions of tile roofs.

Similar to the adhesive-set specimens, four possible failure modes were identified: (1) bonding failure at the interface between the ridge tile and the mortar (2) bonding failure at the interface between the field tiles and the mortar, (3) failure within the mortar, and (4) bearing failure of the tile at the point of load application.

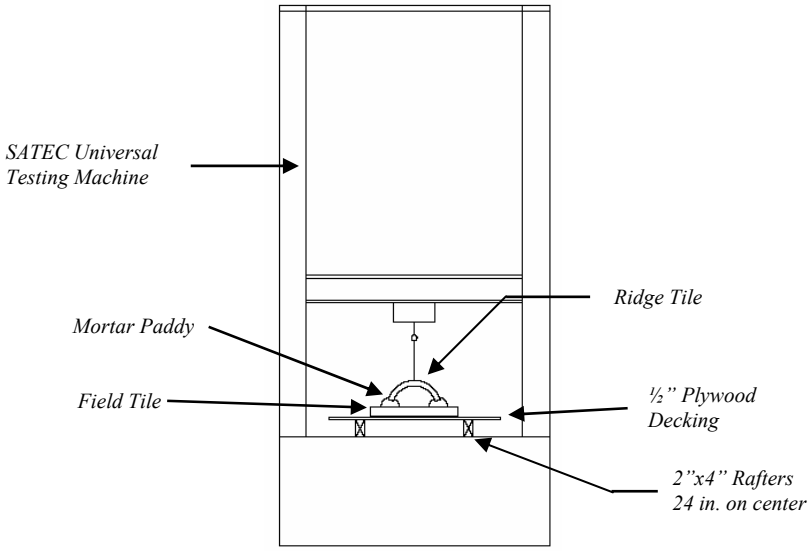

Figure 3.8: Test Apparatus and Set-Up for Roof Tiles with Mortar-Set

3.2.1 Uplift Resistance of Tiles with Mortar-Set Subjected to Center-Point Loading

Three (3) clay and three (3) concrete ridge tile specimens were set up with mortar-set, kept inside the lab at room temperature, and tested 14 days later by pulling only the center tile.

Tables 3.5 and 3.6 list test results for clay and concrete tiles with mortar-set, respectively. Figures 3.9 and 3.10 show typical failure modes for clay and concrete tiles, respectively. The failure load was taken as the load required to cause additional deflection without any further resistance. The average uplift resistance for concrete tiles was found to be 822 lbs. Clay tiles, on the other hand, exhibited bonding failure at the interface between the field tiles and the mortar. The average uplift resistance for clay tiles was only 253 lbs, or 31% of that of concrete tiles.

Table 3.5: Test Results of Clay Tiles with Mortar-Set

Specimen No.	Uplift Resistance (lbs)	Failure Mode
1	430	Debonding of Ridge Tile from Mortar
2	168	Debonding of Field Tile from Mortar
3	160	Debonding of Ridge Tile from Mortar
Average	253	

Table 3.6: Test Results of Concrete Tiles with Mortar-Set

Specimen No.	Uplift Resistance (lbs)	Failure Mode
1	704	Debonding of Ridge Tile from Mortar
2	867	Debonding of Ridge Tile from Mortar
3	894	Debonding of Ridge Tile from Mortar
Average	822	

3.2.2 Uplift Resistance of Ridge Tiles with Mortar-Set Subjected to Three-Point Loading

Two (2) samples of three ridge tile assembly of concrete and clay were set up with mortar-set, kept inside the lab at room temperature, and tested 14 days later by pulling on all three tiles simultaneously.

Tables 3.7 and 3.8 list test results for clay and concrete tiles with mortar-set, respectively. Figures 3.11 and 3.12 show typical failure modes for clay and concrete tiles, respectively. The failure load was taken to be the load required to cause additional deflection without any further resistance. The average uplift resistance for concrete tiles was found to be 565 lbs. Clay tiles, on the other hand, exhibited bonding failure at the interface between the field tiles and the mortar. The average uplift resistance was only 60 lbs, or 11% of that of concrete tiles.

Figure 3.9: Typical Failure Mode of Clay Tiles with Mortar-Set

Figure 3.10: Typical Failure Mode of Concrete Tiles with Mortar-Set

Table 3.7: Test Results of Clay Tiles with Mortar-Set

Specimen No.	Uplift Resistance (lbs)	Failure Mode
1	37	Debonding of Field Tile from Mortar
2	82	Debonding of Field Tile from Mortar
Average	60	

Table 3.8: Test Results of Concrete Tiles with Mortar-Set

Specimen No.	Uplift Resistance (lbs)	Failure Mode
1	509	Debonding of Ridge Tile from Mortar
2	621	Field Tile Broke
Average	565	

Figure 3.11: Typical Failure Mode of Clay Tiles with Mortar-Set

Figure 3.12: Typical Failure Mode of Concrete Tiles with Mortar-Set

3.3 Comparison with Phase 1

The failure load on a single ridge tile obtained in Phase 2 using load-deflection tests (see Section 6) fell within the range of those obtained in Phase 1. This implies that the results from the monotonic uplift tests of both phases are reliable and consistent with each other. A quick comparison between test results obtained for three ridge tile assemblies in this phase with the single ridge tile tests from Phase 1 showed no particular trend. While the concrete with mortar and clay with foam systems exhibited a slight increase in the uplift resistance, the concrete with foam and clay with mortar systems experienced a slight decrease of uplift capacity, as shown in Table 3.9. The difference in the results is within ±8%. Hence, it can be concluded that tile overlap does not contribute in any significant manner to the uplift capacity of the roof tiles.

Table 3.9: Comparison of Test Results

System Type	Phase I (lbs)*	Phase II (lbs)**	% Difference
Clay attached with foam	547	590	7.9%
Clay attached with mortar	178	164	-7.9%
Concrete attached with foam	305	291	-4.6%
Concrete attached with mortar	848	880	3.8%

* Single ridge tile test.

** Three ridge tile assembly; pulling the center tile only.

3.4 Uplift Resistance of Field Tiles

These tests were conducted in order to evaluate the uplift resistance of concrete and clay field tiles attached with adhesive-set or mortar-set systems. The tiles were attached with Polypro AH 160 roof tile adhesive (Figure 3.13) to a hot mopped 30/90 deck underlayment (Figure 3.14). The framing system consisted of a ½" plywood decking mounted on 2"x 4" rafters spaced at 24" on center. A ¼" diameter hole was drilled at 3/4 of the length of the tile along its center line, and a ¼" steel bolt was fastened to the tile to apply an upward force. A 1" washer was placed under the tile to increase the contact area of the applied force in order to avoid failure due to stress concentration.

Figure 3.13: Deck Underlayment System

Figure 3.14: Typical Foam Paddy

Four possible failure modes were identified: (1) bonding failure at the interface between the tile and the foam (2) bonding failure at the interface between the underlayment and the foam, (3) failure within the foam paddy itself, and (4) bearing failure of the tile at the point of load application.

Three (3) clay and three (3) concrete field tile specimens were set up for each of the two attachment systems (adhesive-set and mortar-set), and were kept inside the lab at room temperature. Adhesive-set specimens were tested 5 days after preparation, while mortar-set specimens were allowed to cure for 15 days before testing. Each test specimen

consisted of single field tile attached with adhesive-set to the underlayment. Figure 3.15 shows the test set-up for field tiles.

Tables 3.10−3.13 list the test results for clay and concrete tiles with adhesive-set and mortar-set, respectively. The failure load was taken to be the load required to cause additional deflection without any further resistance.

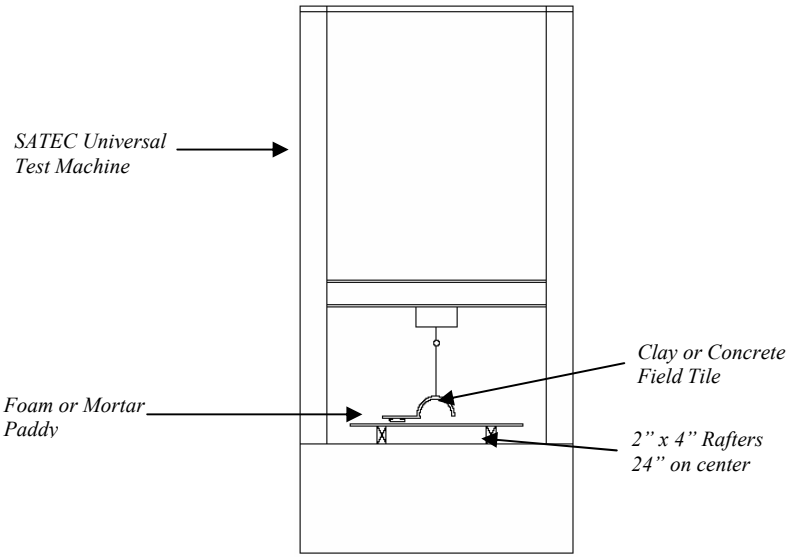

Figure 3.15: Testing Apparatus and Set -Up for Field Tiles with Adhesive-Set or Mortar-Set

Table 3.10: Test Results of Clay Tiles with Adhesive–Set

Specimen No.	Uplift Resistance (lbs)	Failure Mode
1	154	Debonding of Underlayment from Foam
2	143	Debonding of Underlayment from Foam
3	87	Debonding of Underlayment from Foam
Average	128	

Table 3.11 Test Results of Concrete Tiles with Adhesive-Set

Specimen No.	Uplift Resistance (lbs)	Failure Mode
1	139	Debonding of Field Tile from Foam
2	107	Debonding of Field Tile from Foam
3	117	Debonding of Field Tile from Foam
Average	121	

Table 3.12: Test Results of Clay Tiles with Mortar–Set

Specimen No.	Uplift Resistance (lbs)	Failure Mode
1	35	Debonding of Field Tile from Mortar
2	62	Debonding of Field Tile from Mortar
3	77	Debonding of Field Tile from Mortar
Average	58	

Table 3.13: Test Results of Concrete Tiles with Mortar-Set

Specimen No.	Uplift Resistance (lbs)	Failure Mode
1	112	Debonding of Underlayment from Mortar
2	92	Debonding of Underlayment from Mortar
3	120	Debonding of Underlayment from Mortar
Average	108	

Figures 3.16 and 3.17 show typical failure surfaces of clay and concrete tiles with adhesive-set, respectively. Concrete tiles showed bonding failure at the interface between the tile and the adhesive foam. Little or no foam remained bonded to concrete tiles after failure, as shown in Figure 3.17. The average uplift resistance for concrete tiles was 121 lbs. Clay tiles, on the other hand, failed at the interface of the foam and the underlayment. The average uplift resistance for the clay tiles was 128 lbs.

Figure 3.16: Typical Failure Surface of Clay Tiles with Adhesive-Set

Figure 3.17: Typical Failure Surface of Concrete Tiles with Adhesive-Set

Figures 3.18 and 3.19 show the typical failure surfaces of clay and concrete tiles with mortar-set, respectively. Concrete tiles exhibited bonding failure at the interface between the mortar and the underlayment. The average uplift resistance for concrete tiles was found to be 108 lbs. Clay tiles, on the other hand, exhibited failure at the interface between the tile and the mortar. The average uplift resistance for clay tiles was only 58 lbs, or 54% of that of concrete tiles.

Figure 3.18: Typical Failure Surface of Clay Tile with Mortar-Set

Figure 3.19: Typical Failure Surface of Concrete Tile with Mortar-Set

3.5 Cyclic Loading

Monotonic loading used to evaluate tile performance may over-estimate the uplift resistance of tiles, as they neglect the cyclic loading pattern of a hurricane, which may lead to low-cycle fatigue failure of roof tiles. Cyclic load tests were therefore conducted for each of the four roof systems.

Four single ridge tile specimens (one for each type of tile and attachment system) were set up in the same manner as that previously described for monotonic tests. The specimens were then tested by applying and releasing an uplift force equal to 60% of the respective uplift resistance obtained for each roof system in this phase. The 60% limit was chosen as a safe starting point to ensure that the specimens would undergo the fatigue cycles without failing at an early stage. If the specimen did not break after 50 cycles, the applied force was then increased monotonically up to failure.

Using a cycle duration of approximately 30 seconds, only one of the four systems (clay tiles with mortar) failed before all 50 cycles were completed. The other three systems withstood the 50 cycles, as shown in Table 3.14. A quick comparison of these results with those obtained from the monotonic load testing of ridge tiles shows a significant reduction in the uplift resistance of tiles. Table 3.14 shows that monotonic uplift tests overestimate the capacity of roof tile by as much as 40%, depending on the type of

attachment. These results are consistent with the MAT reports that recommend dynamic testing be used in predicting the performance of roof tiles under hurricane conditions.

Table 3.14: Cyclic Load Test Results

System	Monotonic Uplift Capacity (lbs)*	Load Applied for Cyclic Test (lbs)**	Number of Cycles	Residual Uplift Capacity (lbs)‡
Clay with Foam	495	297	50	360
Clay with Mortar	156	94	47***	N/A
Concrete with Foam	287	172	50	381
Concrete with Mortar	693	416	50	620

* From Phase 2.
** 60% of average uplift resistance from Phase 2.
*** Failed after 47 cycles.
‡ From subsequent monotonic load test after 50 cycles.

4.0 Impact Testing

Another factor that affects tile roofs during a hurricane is projectile impact. Even though the density of projectiles impacting a roof may be low, the damage it produces could be significant. The damage that projectile impacts produce on tile roofs is two-fold. On the one hand, the projectile impact damages the tile(s) it comes in contact with along with a number of tiles that lie within a certain radius affected by the transfer of the impact force. On the other hand, the loss of tiles under the direct impact of a projectile causes damage to the integrity of the roof as a system, whereby wind can easily flow under the remaining roof tiles. This results in a domino-like effect causing more and more roof tiles to be lost. Two types of impact tests were conducted to compare the clay and concrete tiles: drop-ball, and air cannon tests.

4.1 Drop-Ball Test

The drop-ball test was designed to compare the impact energy to break clay and concrete tiles. A concrete ball weighing 1.21 lb was dropped on three samples of concrete and clay field tiles. The tiles were placed on a solid flat surface, and the concrete ball was dropped on them from uniformly increasing heights, until the tiles broke. The average heights required for breaking the concrete and clay tiles were obtained from these samples. Since the dropped mass is the same, the ratio of breaking energy is equal to the ratio of the corresponding heights. Figure 4.1 illustrates the procedure.

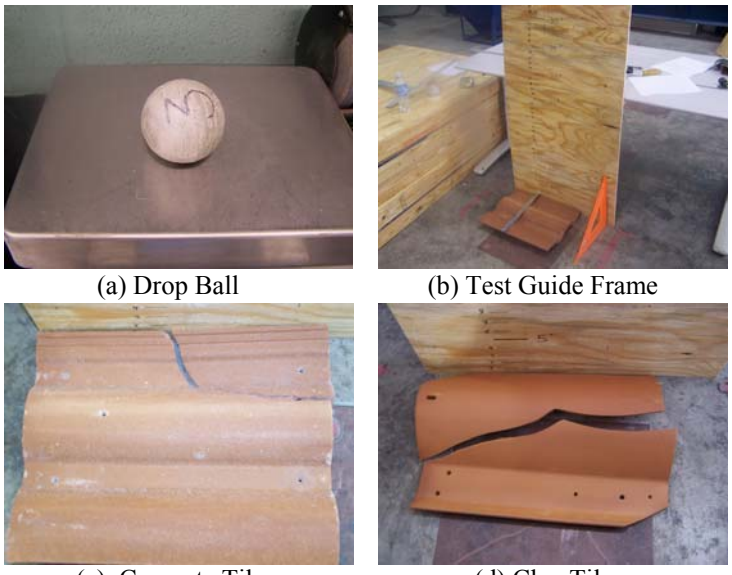

(a) Drop Ball (b) Test Guide Frame

(c) Concrete Tile (d) Clay Tile

Figure 4.1: Drop-Ball Test

The drop-ball tests yielded an average breaking height of 9.5 inches for clay tiles and 13.17 inches for concrete tiles. The ratio of the breaking energy thus obtained was 1.39. This ratio implies that concrete tiles, on average, are 39% stronger in resisting direct projectile impact than clay tiles. The detailed results for the drop-ball tests are shown in Tables 4.1 and 4.2 for clay and concrete tiles, respectively.

Table 4.1: Clay Tiles Drop-Ball Test Results

			Test 1	Test 2	Test 3
Height of Ball (in)	**Height of Tile (in)**	**Drop Height (in)**	**Tile After Impact**	**Tile After Impact**	**Tile After Impact**
9	3.5	5.5	ok	ok	ok
10	3.5	6.5	ok	ok	ok
11	3.5	7.5	ok	**Broke**	ok
12	3.5	8.5	ok	----	ok
13	3.5	9.5	ok	----	ok
14	3.5	**10.5**	**Broke**	----	**Broke**
15	3.5	-----	----	----	
16	3.5	-----	-----	----	
			Average =	**9.5**	in

Table 4.2: Concrete Tiles Drop-Ball Test Results

			Test 1	Test 2	Test 3
Height of Ball (in)	**Height of tile (in)**	**Drop Height (in)**	**Tile After Impact**	**Tile After Impact**	**Tile After Impact**
9	2.5	6.5	ok	ok	ok
10	2.5	7.5	ok	ok	ok
11	2.5	8.5	ok	ok	ok
12	2.5	9.5	ok	ok	ok
13	2.5	10.5	ok	ok	ok
14	2.5	11.5	ok	ok	ok
15	2.5	12.5	**Broke**	ok	ok
16	2.5	13.5		**Broke**	**Broke**
			Average =	**13.17**	in

4.2 Air Cannon Impact Test

Two experiments were conducted using an air cannon projectile fired at concrete and clay roof tiles. The first experiment was performed using a single field tile, and the second using a full-scale roof section. The purpose of the first experiment was to determine whether there was a difference in the failure mode of the two types of tiles, when impacted by a projectile during a hurricane. The purpose of the second experiment was to determine the extent of damage suffered by each of these two types of roof tiles when impacted by a projectile during a hurricane.

In the first experiment, three individual samples of clay and concrete field tiles were attached to a ½" piece of plywood deck using the same mechanical attachment system, as described in the Section 3. The plywood deck was in-turn mounted on 2"x 4" rafters spaced at 24" on center. The specimens were placed on a wooden frame with a 4:12 slope (typical of residential roofs) placed at 32 ft away from the air cannon, as shown in Figure 4.2. A 3 ft piece of 2"x 4" Southern Pine lumber was used as the projectile in these experiments.

Figure 4.2: Air Cannon Impact Test for Single Field Tiles

The experiments showed that both concrete and clay field tiles would fail under the impact of the 2"x 4" lumber at 5 psi cannon air pressure – the lowest readable pressure on the gage. What was interesting in the results of this test is the mode of failure for each type of tile. While concrete tiles only broke in half (Figure 4.3), clay tiles were totally shattered by the impact with very little remaining on the plywood deck (Figure 4.4).

Figure 4.3: Single Concrete Field Tile After Projectile Impact

Figure 4.4: Single Clay Field Tile After Projectile Impact

The second type of air cannon projectile impact tests was performed on the full-scale tile roof section, which was built for the WoW hurricane simulation tests described in Section 5. In this experiment, Testing Application Standard (TAS) 201-94 Impact Test Procedures was followed. The projectile used was a 9 lb solid S4S nominal 2" x 4" #2 surface dry Southern Pine, as specified by Section 1626.2.3 of the FBC. A sabot was attached to the trailing edge of the missile to facilitate launching.

After the WoW hurricane simulation test for a tile roof system was complete, the cannon was set up at 15 ft from the point of impact, which was a 5" radius at the center of the roof (FBC Section 1626.2.5). The cannon was then raised 6" above the height of the impact point to account for drop of the missile as it travels in the air. The sabot and the 9 lb 2" x 4" projectile were loaded into the cannon nozzle. Compressed air was driven into

the cannon barrel to pressurize it up to 15 psi. This pressure drives the projectile to an impact velocity of 50 ft/sec (15.2 m/sec) as required by the FBC Section 1626.2.4.

Two roof systems were tested in this experiment: concrete tile with mortar and clay tile with foam. These two tile roof systems were tested for impact out of the 4 WoW tests for two main reasons: first, they were the two tile roof systems that proved to have the highest performance in the mechanical uplift tests; and second, they were the two roof systems that survived the WoW testing with a significant area of tiles undamaged by the wind.

Figure 4.5 shows the concrete tiles with mortar absorbed the impact of the projectile to a large extent while sustaining minimal damage. The roof tiles in the impact area were damaged, but no tiles flew off of the roof. Figure 4.6 shows the clay tiles with foam sustained extensive damage in and around the impact area. Many of the clay tiles were launched into the air as projectiles upon impact. The damage shown in Figure 4.5 however, is not entirely the result of the projectile impact. Initial damage amounting to about 13 tiles was caused by the WoW test. Figure 4.7 shows several photographic frames for air cannon impact tests of concrete tiles.

Figure 4.5: Impact Test on Concrete with Mortar Tile Roof System

Figure 4.6: Impact Test on Clay with Foam Tile Roof System

The following can be concluded from the results of the three impact tests conducted in this part of the study:

1. Concrete tiles are 39% stronger than clay roof tiles in resisting impact by a projectile during a hurricane;
2. Concrete tiles tend to break when impacted by a speeding projectile, while clay tiles tend to shatter into very small pieces; and
3. Concrete tiles with mortar absorb the impact of projectiles locally, while clay tiles with foam tend to sustain extensive damage to a significant area around the impact zone.

(1)

(2)

(3)

(4)

Figure 4.7: Air Cannon Impact Test of Concrete Tiles (Frames 1-4)

5.0 Wall of Wind (WOW) Testing

Unlike conventional wind tunnel studies and destructive testing procedures, the one-of-a-kind Wall of Wind (WoW) apparatus simulates the actual dynamics of wind impinging on a low-rise structure at full-scale, and allows coupling of wind flow with material response.

Testing for this part of the project took place at the Florida International University Engineering Campus using the 2-fan Wall of Wind (WoW) testing facility (Figure 5.1), funded by the Florida Division of Emergency Management (FLDEM). The 2-fan WoW measures 16 ft tall and 8 ft wide, and is capable of generating maximum wind speeds of 125 mph (56 m/s), which represents Category 2-4 hurricane winds on the Saffir-Simpson scale.

The 2-fan WoW is used in this project to: (1) compare pressure coefficients for four sets of tile roofs (i.e., clay tiles with foam, clay tiles with mortar, concrete tiles with foam, and concrete tiles with mortar) with ASCE 7-05 and use them in the subsequent FEM analysis; and (2) compare the performance of different tile roof systems under simulated hurricane impact.

Figure 5.1: 2-Fan WoW System

5.1 Wall of Wind Test Facility

The following sections provide a detailed description of the equipment and instrumentation used in part of this project.

5.1.1 WoW System Controls

The two engines of the WoW system were simultaneously controlled using the apparatus developed by PrimeTest Automation (Figure 5.2). The wind speed was controlled using

the pre-calibration curves of generated wind speed with the engine speed (RPM).

5.1.2 Data Acquisition

The data acquisition (DAQ) system for the WoW tests was also developed by PrimeTest Automation using the LabView software (Figure 5.3) and was operated at a sampling rate of 100 Hz. Pressure transducers were calibrated using the DAQ based on known pressures generated by a hand-held Omega PCL-200C calibration kit. The calibration curves were then incorporated into the DAQ software.

Figure 5.2: 2-Fan WoW Control System

Figure 5.3: DAQ System for WoW Testing

5.1.3 Pressure Transducers

Thirty-two (32) Setra model 265 very low differential pressure transducers were used to measure the negative pressures on the roof induced by a simulated hurricane wind flow (Figure 5.4). Each transducer had two ports: a reference port for ambient pressure, and a port connected to the test structure to measure the fluctuating pressures on the roof. The result was a differential pressure, measured first as a voltage ranging from 0-5 V and then converted into psi (pounds per square inch). The transducers had a pressure range of ±1.8 psi (±260 psf), and transmitted data at a frequency of 10 Hz and an accuracy of ±1 %.

The ports on the pressure transducers were connected to the reference point and the roof using a system of tubing. The reference pressure measurement was taken in a pressure pit located approximately 50 ft away from the test structure. A 3 in. PVC pipe was extended from the pressure pit into the test structure and was then reduced to a 3/4 in. PVC pressure manifold (Figures 5.5 and 5.6). The pressure manifold distributed the reference

pressure to 32 different PVC ball valves. Each PVC ball valve was connected to a 3/16 in. ID (inside diameter) polyurethane tubing. The polyurethane tubing was in-turn connected to a 20-ft long silicon tubing with 1/16 in. ID (inside diameter) via a plastic reduction fitting. This 1/16 in. ID tubing was then attached to the reference pressure port using another piece of 3/16 in. ID polyurethane tubing, as shown in Figure 5.7. The small silicon tubing was used to filter out any noise cause by the resonance of the tubing, and is therefore referred to as restrictor tubing.

Figure 5.4: Pressure Transducer

Figure 5.5: 3-in. PVC Pipe from Reference Pressure Line

Figure 5.6: PVC Reference Pressure Manifold

The tubing system for the dynamic pressure port was set up in the following manner. The 3/16 in. ID polyurethane tubing was connected to a 1/4 in. OD (outside diameter) copper pressure tap, which extended from the roof tiles, as shown in Figure 5.8. The total length of tubing that ran from the roof tap to the pressure port was normally restricted to 12 in., with a maximum length of 16 in., to avoid distorted measurements.

The extensive tubing system needed for the pressure transducers required 2 types of calibration, standard and dynamic. These calibrations were performed to ensure accuracy in the measurement, as presented in detail in [Blessing, 2007].

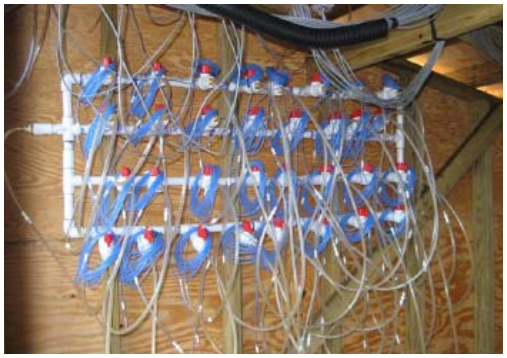

Figure 5.7: Reference Pressure Line with Restrictor Tubing Attached

Figure 5.8: Roof Pressure Line

5.2 Experimental Setup

5.2.1 WoW Test Structure and Tile Roofs

All testing for this experiment was done using a scaled test structure measuring 8 ft x 8 ft in plan, and 10.7 ft in height (Figure 5.9). The test structure had a monoslope with a pitch of 18.4°, and was not enclosed from the back side.

The test structure was placed 6 ft from the edge of the 2-fan WoW, as shown in Figure 5.10. This distance allowed the flow to develop while keeping the structure close enough to the source of the flow, so that it would still experience high velocity winds.

The plywood structure was designed to withstand the maximum wind speed generated by the WoW. On the top of the structure, four sets of tile roofs (Figure 5.10) were built by a licensed professional roofer, as follows:

(1) Clay tiles with foam;
(2) Clay tiles with mortar;
(3) Concrete tiles with foam; and
(4) Concrete tiles with mortar.

For the clay tiles with foam, two models were built. The only difference between these two models was that there were extra ridge tiles placed on the sides of the roof for the second model.

The measurements were made at two typical wind directions: 0° and 50° angles of attack with respect to the line normal to the eave, as shown in Figure 5.11.

Windward Side

Leeward Side

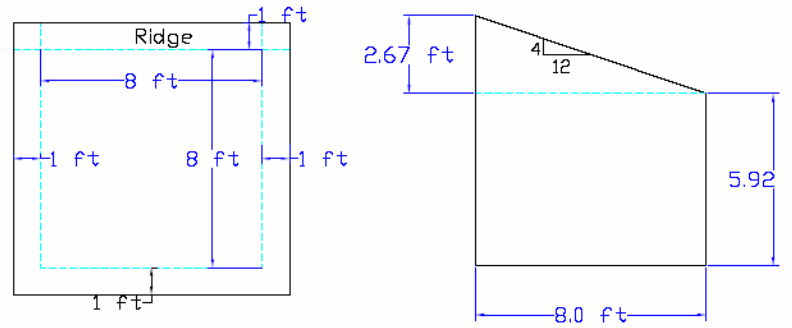

Plan

Elevation

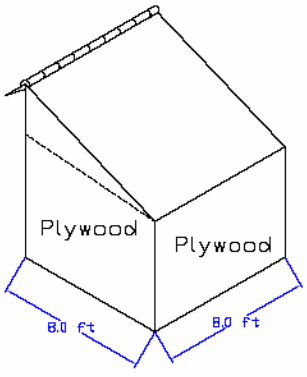

Perspective

Figure 5.9: WoW Scaled Test Structure

(a) Model 1a: Clay Roof Tiles with Foam

(b) Model 1b: Clay Tile Roof with Foam and Extra Side Ridge Tiles

(c) Model 2: Clay Roof Tiles with Mortar

(d) Model 3: Concrete Roof Tiles with Foam

(e) Model 4: Concrete Roof Tiles with Mortar

Figure 5.10: Tile Roof Test Models

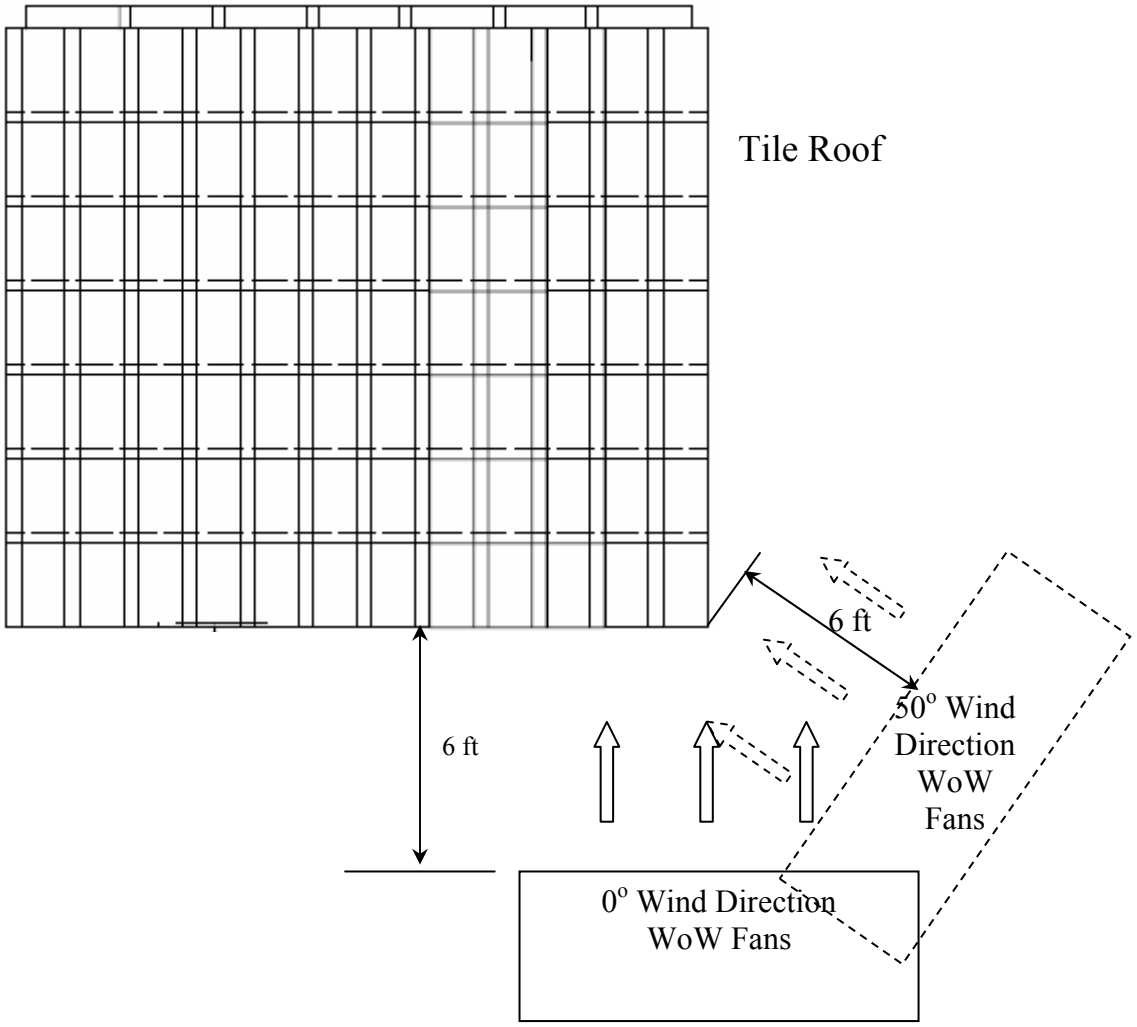

Figure 5.11: Wind Direction and Layout of WoW Fans

5.2.2 Testing Wind Speed, Sampling Frequency, and Duration

Each roof model was tested at two wind speeds of 60 and 120 mph for each wind direction. Because the wind flow at 120 mph speed decays rapidly over a given length, the wind speed of 120 mph was mainly used to check the performance of roof tiles in a simulated hurricane condition.

A Pitot tube was used to measure the wind speed in front of the test structure, as shown in Figure 5.12. The tube was set up at a height of 6 ft, corresponding to the eave height of the test roof. The wind speed measured was later used to calculate the pressure coefficients on the roof tiles.

Data for each test was recorded for a duration of 6 min at a sampling rate of 100 Hz.

Figure 5.12: Pitot Wind Tube for Measuring Wind Speed

5.2.3 Layout of the Pressure Taps

A total of 32 pressure taps were drilled into the clay roof tiles with either foam or mortar, as shown in Figure 5.13. The coordinates of each pressure tap are listed in Table 5.1. The distribution of the pressure taps were as follows: 5 field tiles with 4 pressure taps each; 6 field tiles with 1 pressure tap each; and 2 ridge tiles with 3 pressure taps each.

Table 5.1: Pressure Taps Coordinates for Clay Tile Roofs

Points	X *	Y*	Points	X*	Y*	Points	X*	Y *
1	58.75	8	12	1.25	8	23	3.75	72
2	56.25	8	13	58.75	24	24	53.75	105
3	53.75	8	14	56.25	24	25	23.75	105
4	51.25	8	15	53.75	24	26	3.75	105
5	28.75	8	16	51.25	24	27	52.5	120.8
6	26.25	8	17	8.75	24	28	52.5	118.3
7	23.75	8	18	6.25	24	29	52.5	115.8
8	21.25	8	19	3.75	24	30	7.5	120.8
9	8.75	8	20	1.25	24	31	7.5	118.3
10	6.25	8	21	53.75	72	32	7.5	115.8
11	3.75	8	22	23.75	72			

* Coordinates in inches from the lower right corner of the roof.

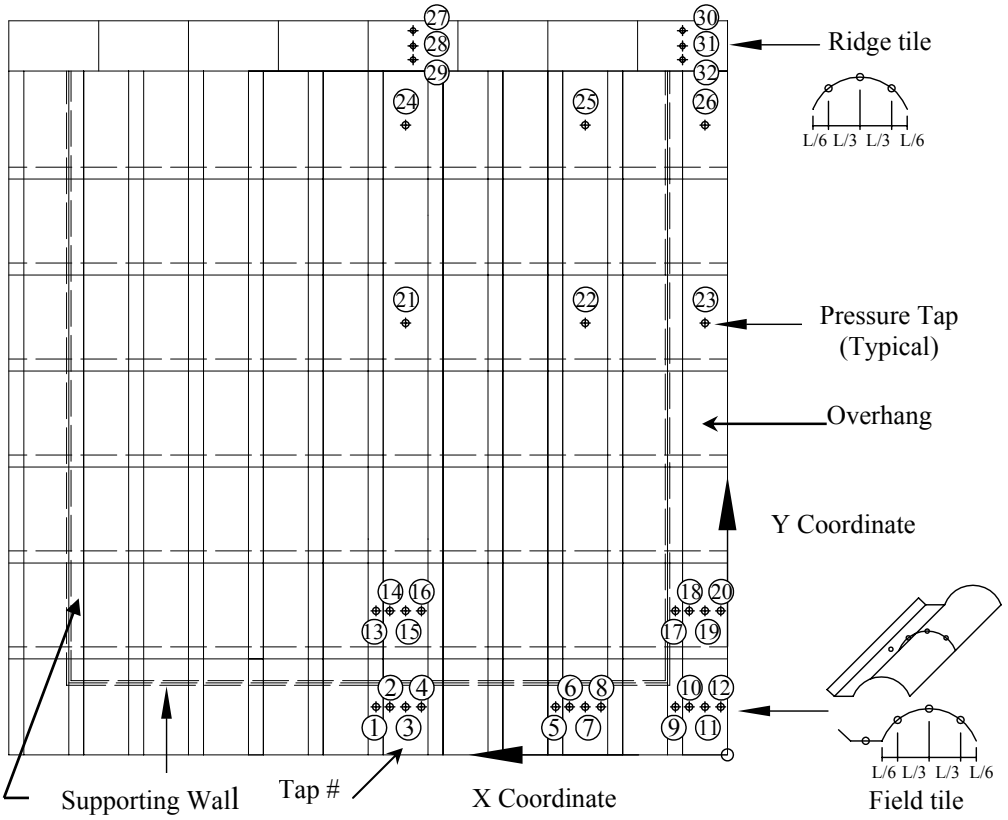

Figure 5.13: Pressure Taps Layout for Clay Tile Roofs

A total 32 pressure taps were drilled into the concrete roof tiles with either foam or mortar, as shown in Figure 5.14. The coordinates of each pressure tap are listed in Table 5.2. The distribution of the pressure taps were as follows: 2 field tiles with 4 pressure taps each; 1 field tile with 3 pressure taps; 2 field tiles with 2 pressure taps each; 11 field tiles with 1 pressure tap each; and 2 ridge tiles with 3 pressure taps each.

Table 5.2: Pressure Taps Coordinates for Concrete Tile Roofs

Points	X*	Y*	Points	X*	Y*	Points	X*	Y*
1	35	7	12	5	21	23	32	91
2	32	7	13	2	21	24	2	91
3	29	7	14	32	35	25	32	106
4	26	7	15	29	35	26	2	106
5	11	7	16	2	35	27	37.5	120.8
6	8	7	17	32	49	28	37.5	118.3
7	5	7	18	2	49	29	37.5	115.8
8	2	7	19	32	63	30	7.5	120.8
9	32	21	20	2	63	31	7.5	118.3
10	29	21	21	32	77	32	7.5	115.8
11	8	21	22	2	77			

* Coordinates in inches from the lower right corner of the roof.

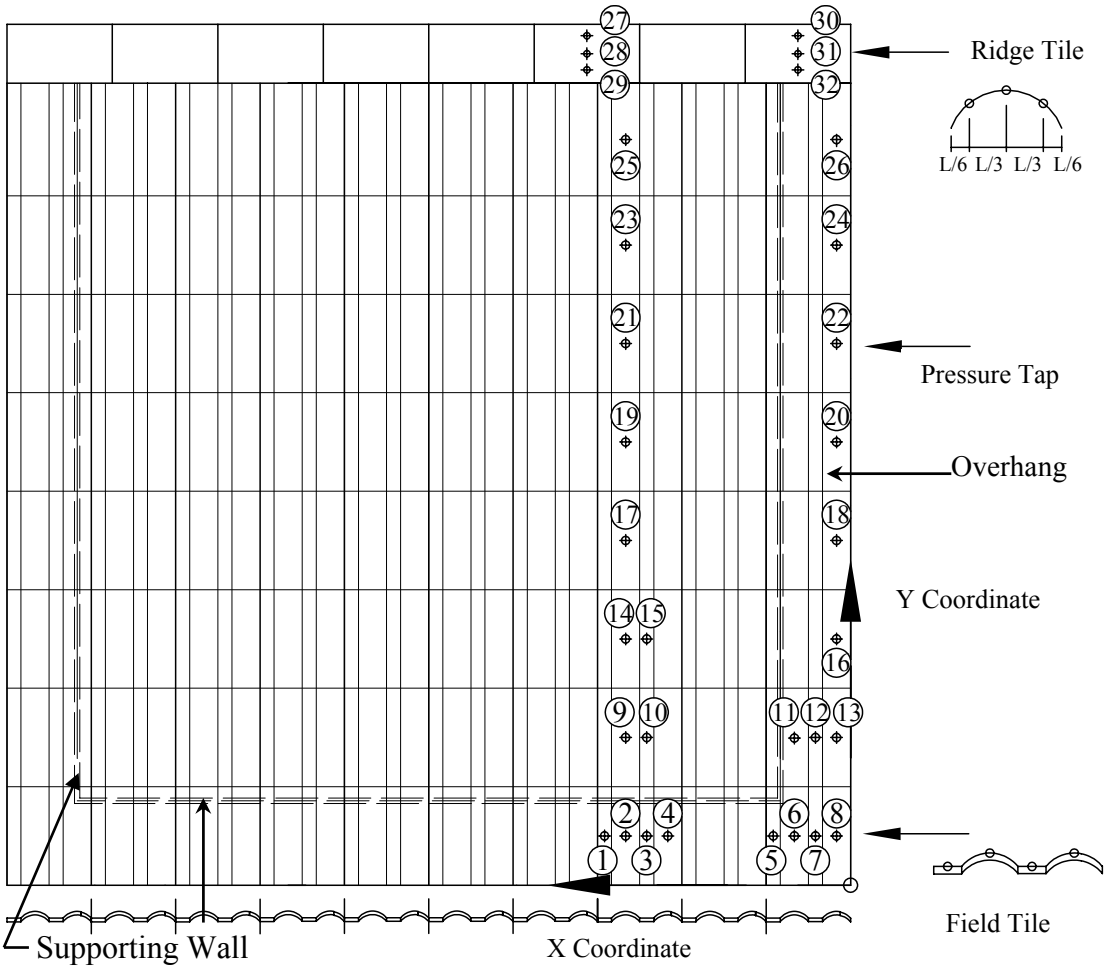

Figure 5.14: Pressure Taps Layout for Concrete Tile Roofs

5.2.4 Definition of Pressure Coefficients

The pressure coefficient, C_{Pi}, can be computed as:

$$C_{Pi} = \frac{\Delta P_i}{\frac{1}{2}\rho U^2} \tag{5.1}$$

where C_{Pi} is the pressure coefficient at the i^{th} measured tap; ΔP_i is the differential pressure at the i^{th} measured tap; ρ is the air density; and U is the wind velocity. The mean, RMS (root mean square), and the minimum values of C_{Pi} are computed, as follows:

$$C_{Pmean} = \frac{\sum_1^N C_{Pi}}{N} \tag{5.2}$$

$$C_{\mathrm{P}RMS} = \sqrt{\frac{\sum_1^N \left(C_{Pi} - C_{Pmean}\right)^2}{N-1}} \tag{5.3}$$

$$C_{P\min} = \min\left(C_{Pi}\right) \tag{5.4}$$

where N is the total number of samples in each data set.

5.3 WoW Test Results

5.3.1 Model 1a – Clay Tiles with Foam

This roof system was first tested at 60 mph wind speed in the 0° direction for 6 minutes. No tile damage was visible at the end of this stage. The wind speed was then increased to 120 mph, and was maintained for another 6 minutes. During this stage, some tiles at the windward edge failed (Figure 5.15a). The 2-fan WoW was then oriented along the 50^{o} angle, and the above test procedure was repeated. More roof tiles failed at this stage, as shown in Figure 5.15b.

The failure initiated at the eave and rapidly extended upward, until about 50% of the roof tiles were removed, as can be seen in Figure 5.16.

The pressure coefficients (C_{Pmean}, $C_{\mathrm{P}RMS}$ and $C_{P\min}$) for each pressure tap at 60 mph wind speed in the 0° direction are listed in Table 5.3. The pressure time histories of some typical positions (Points 5, 6, 7, 8 and 31) are shown in Figure 5.17.

(a) Roof Condition Subjected to 120 mph Wind Speed at 0^{o} Direction

(b) Roof Condition Subjected to 120 mph Wind Speed at 50^{o} Direction

Figure 5.15: Failure of Clay-with-Foam Tile Roof System

Figure 5.16: Failure Progress of Clay-with-Foam Tile Roof System (120 mph Wind Speed at 0^{o} Direction)

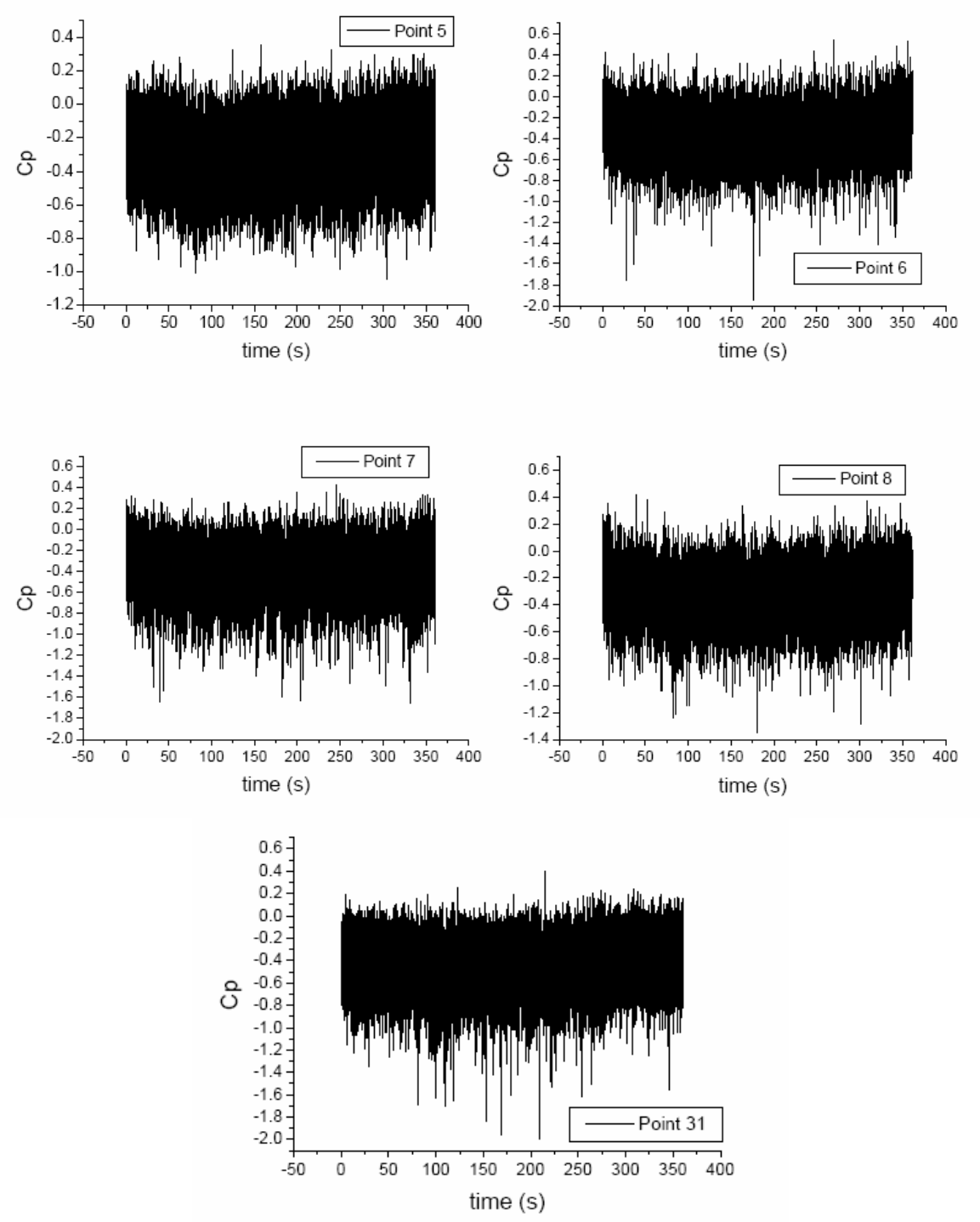

Figure 5.17: Pressure Time Histories for Model 1a
(60 mph Wind Speed at 0^o Direction)

Table 5.3: Pressure Coefficients (C_{Pmean}, $C_{P\,RMS}$ and $C_{P\min}$) of Clay Tile Roofs

(60 mph Wind speed at 0° Direction)

Points	Model 1a			Model 1b			Model 2		
	C_{Pmean}	$C_{\Pr ms}$	$C_{P\min}$	C_{Pmean}	$C_{\Pr ms}$	$C_{P\min}$	C_{Pmean}	$C_{\Pr ms}$	$C_{P\min}$
1	-0.13	0.13	-0.68	-0.37	0.14	-1.03	-0.44	0.20	-1.52
2	-0.25	0.19	-1.59	-0.23	0.21	-1.26	-0.29	0.22	-1.35
3	-0.07	0.21	-2.24	-0.10	0.20	-1.79	-0.23	0.29	-1.92
4	-0.01	0.20	-1.42	-0.23	0.21	-1.61	-0.44	0.18	-1.53
5	-0.30	0.17	-1.04	-0.55	0.17	-1.50	-0.63	0.14	-1.24
6	-0.36	0.21	-1.95	-0.44	0.18	-1.53	-0.49	0.18	-1.69
7	-0.38	0.22	-1.66	-0.49	0.21	-2.27	-0.45	0.23	-1.54
8	-0.33	0.18	-1.35	-0.52	0.16	-1.43	-0.51	0.21	-1.60
9	-0.05	0.20	-0.93	-0.24	0.25	-1.24	-0.23	0.14	-0.82
10	-0.41	0.32	-1.92	-0.24	0.33	-2.31	-0.18	0.28	-2.09
11	-0.15	0.39	-1.62	-0.12	0.41	-1.58	-0.19	0.36	-1.43
12	-0.45	0.16	-1.41	-0.47	0.22	-1.71	-0.28	0.21	-1.54
13	-0.04	0.12	-0.48	-0.03	0.10	-0.65	—	—	—
14	-0.37	0.29	-1.45	-0.17	0.34	-1.55	—	—	—
15	-0.06	0.13	-0.73	-0.11	0.14	-0.83	-0.16	0.11	-0.71
16	-0.24	0.13	-1.09	-0.21	0.11	-0.76	—	—	—
17	0.00	0.13	-0.46	0.06	0.13	-0.50	0.03	0.16	-0.66
18	-0.05	0.14	-0.74	-0.09	0.14	-0.90	-0.11	0.18	-0.85
19	0.11	0.16	-1.06	-0.10	0.15	-1.28	-0.12	0.15	-0.97
20	-0.20	0.15	-1.13	-0.30	0.15	-1.01	-0.11	0.13	-0.85
21	0.18	0.11	-0.11	-0.15	0.12	-0.75	-0.07	0.13	-0.84
22	0.15	0.14	-0.54	0.06	0.12	-0.40	0.05	0.10	-0.30
23	0.11	0.13	-0.46	-0.04	0.12	-0.57	-0.06	0.12	-0.70
24	-0.17	0.13	-0.71	-0.23	0.11	-0.72	0.09	0.10	-0.28
25	-0.34	0.16	-1.03	-0.23	0.14	-0.88	-0.16	0.12	-0.70
26	-0.08	0.14	-0.82	-0.17	0.12	-0.89	-0.26	0.12	-0.78
27	-0.10	0.14	-0.81	-0.56	0.19	-1.55	—	—	—
28	-0.26	0.13	-0.81	-0.36	0.12	-0.93	—	—	—
29	0.51	0.14	0.06	0.19	0.12	-0.37	—	—	—
30	-0.25	0.19	-1.11	-0.48	0.19	-1.30	—	—	—
31	-0.45	0.22	-2.00	-0.50	0.21	-1.74	—	—	—
32	0.41	0.12	-0.01	0.13	0.13	-0.64	—	—	—

5.3.2 Model 1b – Clay Tiles with Foam and Extra Ridge Tiles

This roof system was first tested at 60 mph wind speed in the 0° direction for 6 minutes. No tile damage was visible at the end of this stage. The wind speed was then increased to 120 mph, and after $3^{1/2}$ minutes, a few tiles at the windward edge failed. The other tiles

along the line of wind direction failed subsequently. Lastly, the ridge tiles failed under the impact of the flown field tiles (Figure 5.18a).

The 2-fan WoW was then oriented along the 50^o angle, and the above test procedure was repeated. More roof tiles failed at this stage, as shown in Figure 5.18b. The failure pattern of the roof tiles was observed to be the same as that of Model 1a, as can be seen in Figure 5.19.

The pressure coefficients (C_{Pmean}, $C_{\mathrm{P}RMS}$ and $C_{P\min}$) for each pressure tap at 60 mph wind speed in the 0° and 50^o directions are listed in Tables 5.3 and 5.4, respectively. The pressure time histories of some typical positions (Points 5, 6, 7, 8 and 31) are shown in Figure 5.20. Some tiles failed at 120 mph wind speed. The pressure time histories of some of the taps on the failing tiles (Points 5, 6, 8 and 27) are shown in Figure 5.21.

(a) Roof Conditions Subjected to 120 mph Wind Speed at 0^O Direction

(b) Roof Conditions Subjected to 120 mph Wind Speed at 50^O Direction

Figure 5.18: Failure of Clay-with-Foam Tile Roof System with Extra Ridge Tiles on the Side

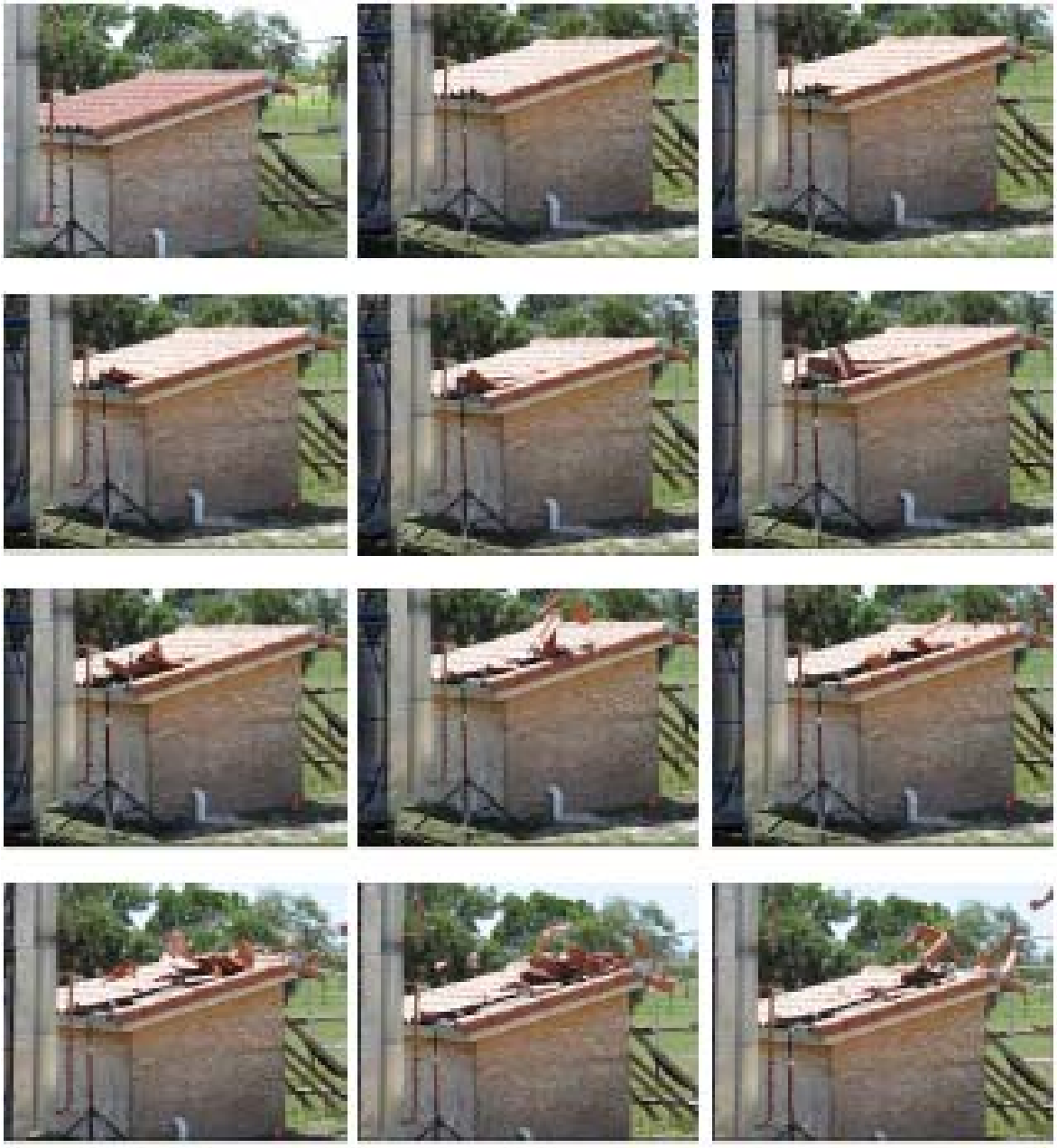

Figure 5.19: Failure Progress of Clay-with-Foam Tile Roof System, Model 1b (120 mph Wind Speed at 0^{o} Direction)

Table 5.4: Pressure Coefficients (C_{Pmean}, $C_{\Pr ms}$ and $C_{P\min}$) of Clay Tile Roofs (60 mph Wind Speed at 50° Direction)

Points	Model 1b			Model 2		
	C_{Pmean}	$C_{\Pr ms}$	$C_{P\min}$	C_{Pmean}	$C_{\Pr ms}$	$C_{P\min}$
1	-0.45	0.13	-1.00	—	—	—
2	-0.28	0.18	-1.02	—	—	—
3	-0.12	0.17	-0.96	—	—	—
4	-0.33	0.13	-0.84	—	—	—
5	—	—	—	-0.34	0.29	-1.77
6	—	—	—	-0.22	0.20	-1.52
7	—	—	—	-0.92	0.29	-2.38
8	—	—	—	0.18	0.33	-1.36
9	-0.18	0.42	-1.85	-0.03	0.24	-0.77
10	**-1.30**	**0.49**	**-3.74**	-0.44	0.45	-3.16
11	-1.39	0.43	-2.78	-1.05	0.44	-2.47
12	-0.77	0.42	-2.52	-0.82	0.22	-1.92
13	-0.16	0.11	-0.75	—	—	—
14	-0.28	0.35	-1.40	—	—	—
15	-0.59	0.21	-1.43	—	—	—
16	-0.23	0.11	-0.65	—	—	—
17	0.19	0.21	-0.67	0.23	0.42	-1.23
18	-0.70	0.25	-2.17	-0.49	0.34	-2.40
19	-0.80	0.18	-1.52	-1.20	0.33	-2.42
20	-0.60	0.31	-2.06	-0.40	0.18	-1.07
21	0.02	0.12	-0.44	—	—	—
22	—	—	—	—	—	—
23	-0.10	0.15	-0.80	-0.04	0.12	-0.67
24	-0.32	0.09	-0.63			
25	-0.23	0.13	-0.88			
26	-0.13	0.11	-0.55	-0.23	0.12	-0.67

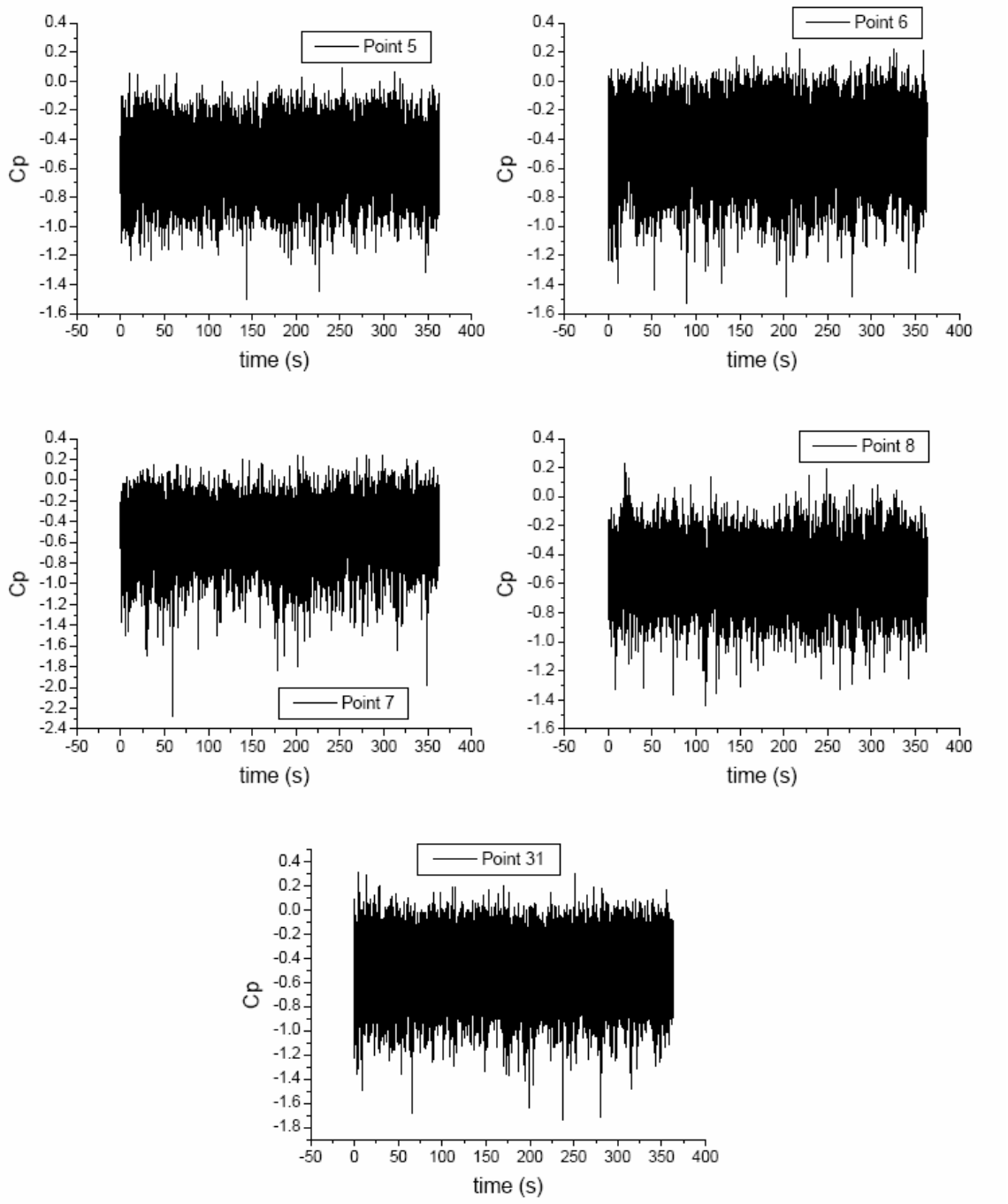

Figure 5.20: Pressure Time Histories for Model 1b
(60 mph Wind Speed at 0^o Direction)

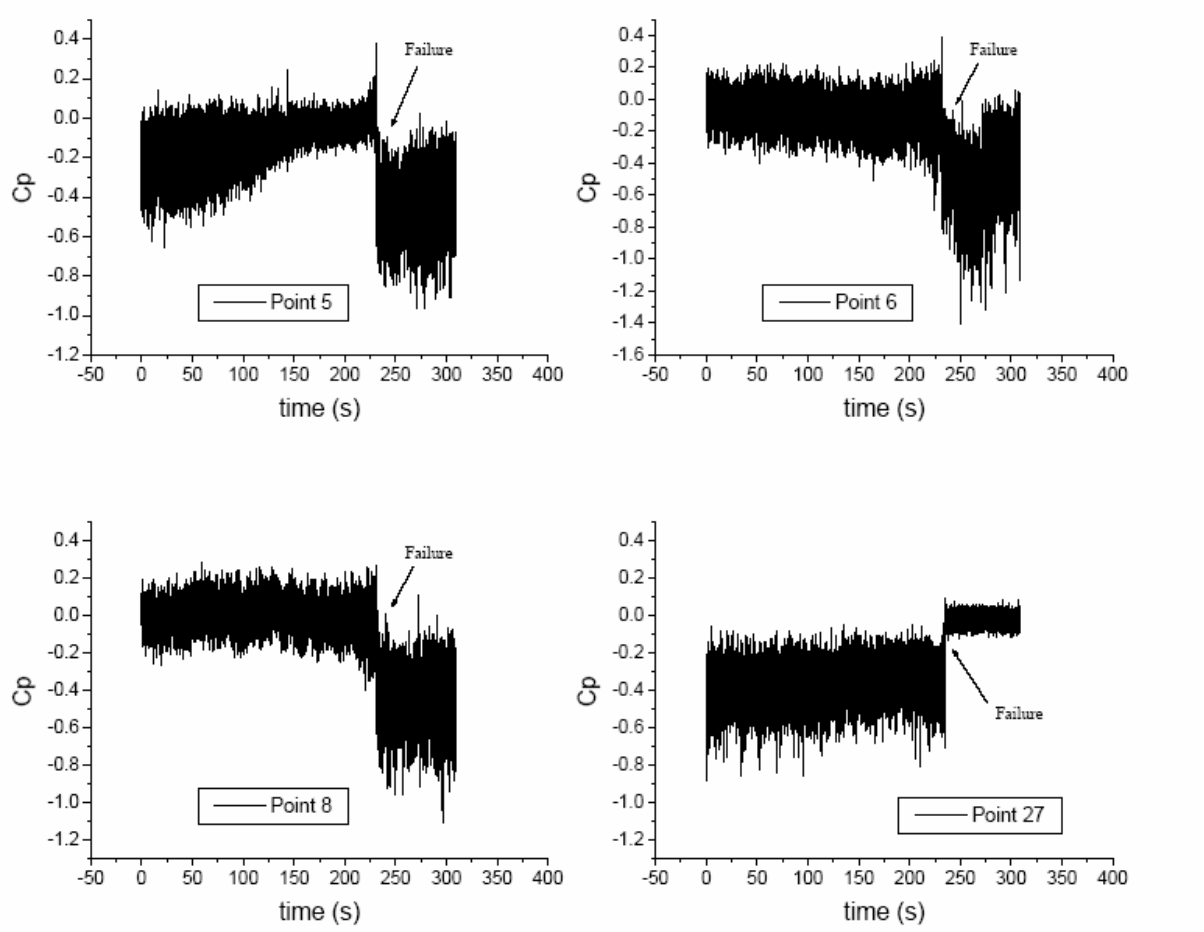

Figure 5.21: Pressure Time Histories for Model 1b
(120 mph Wind Speed at 0° Direction)

5.3.3 Model 2 – Clay Tiles with Mortar

This roof system was first tested at 60 mph wind speed in the 0° wind direction for 6 minutes. No tile damage was visible at the end of this stage. The wind speed was then increased to 120 mph, and after $2^{1/2}$ minutes, a few tiles at the windward edge failed. The other tiles along the line of wind direction failed subsequently. Lastly, the ridge tiles failed under the impact of the flown field tiles (Figure 5.22a).

The 2-fan WoW was then oriented along the 50° angle and the above test procedure was repeated. More roof tiles failed at this stage, as shown in Figure 5.22b. The failure pattern of the roof tiles was observed to be the same as that of Models 1a and 1b, as shown in Figure 5.23.

The pressure coefficients (C_{Pmean}, C_{PRMS} and $C_{P\min}$) for each pressure tap at 60 mph wind speed in the 0° and 50° directions are listed in Tables 5.3 and 5.4, respectively. The pressure time histories of some typical positions (Points 5, 6, 7, and 8) are shown in

Figure 5.24. Some tiles failed at 120 mph wind speed. The pressure time-histories of some of the taps on the failing tiles (Points 1, 2, 3 and 4) are shown in Figure 5.25.

(a) Roof Conditions Subjected to 120 mph Wind Speed at 0^{O} Direction

(b) Roof Conditions Subjected to 120 mph Wind Speed at 50^{O} Direction

Figure 5.22: Failure of Clay-with-Mortar Tile Roof System

Figure 5.23: Failure Progress of Clay-with-Mortar Tile Roof System (120 mph Wind Speed at 0^{o} Direction)

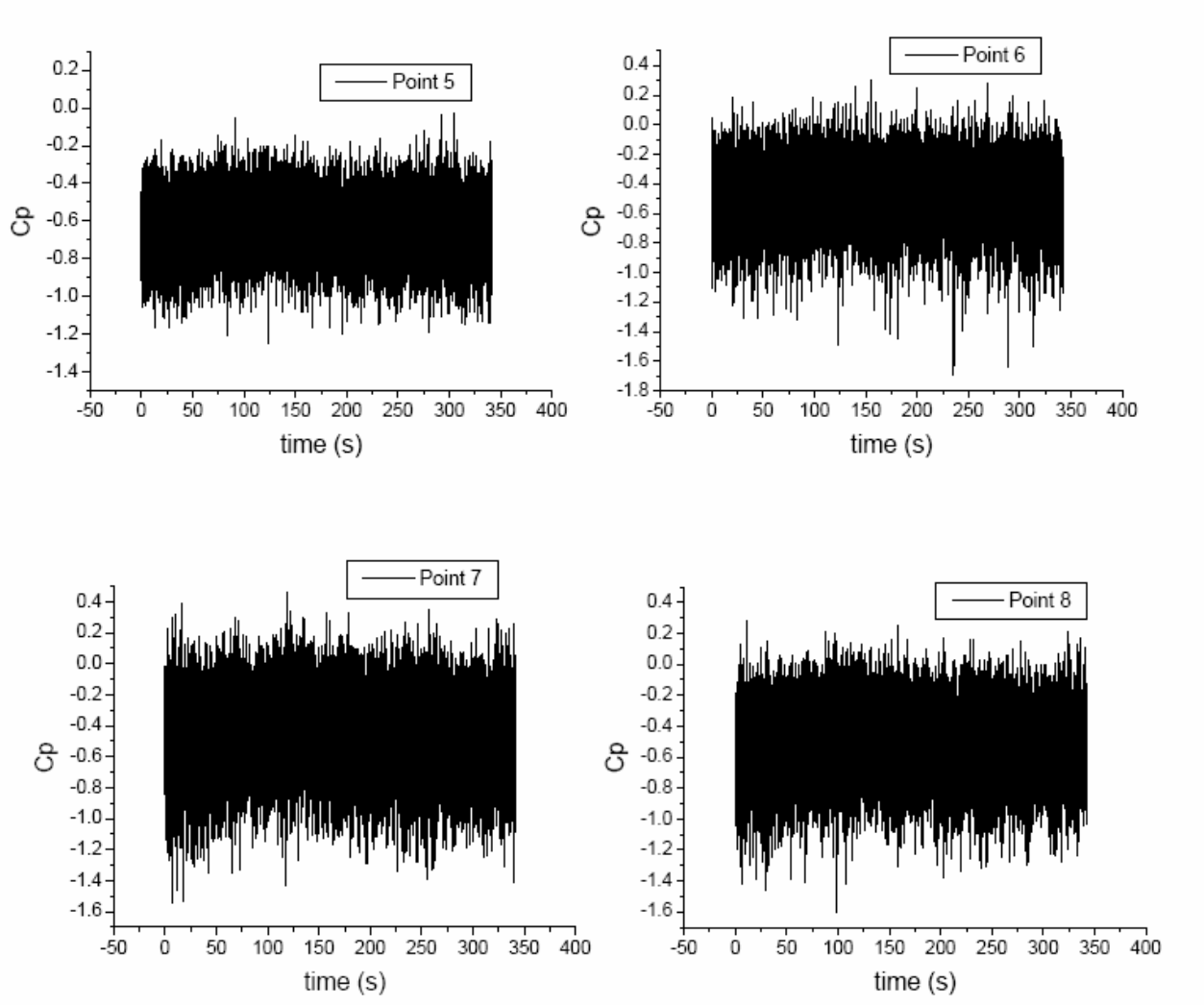

Figure 5.24: Pressure Time Histories for Model 2
(60 mph Wind Speed at 0^o Direction)

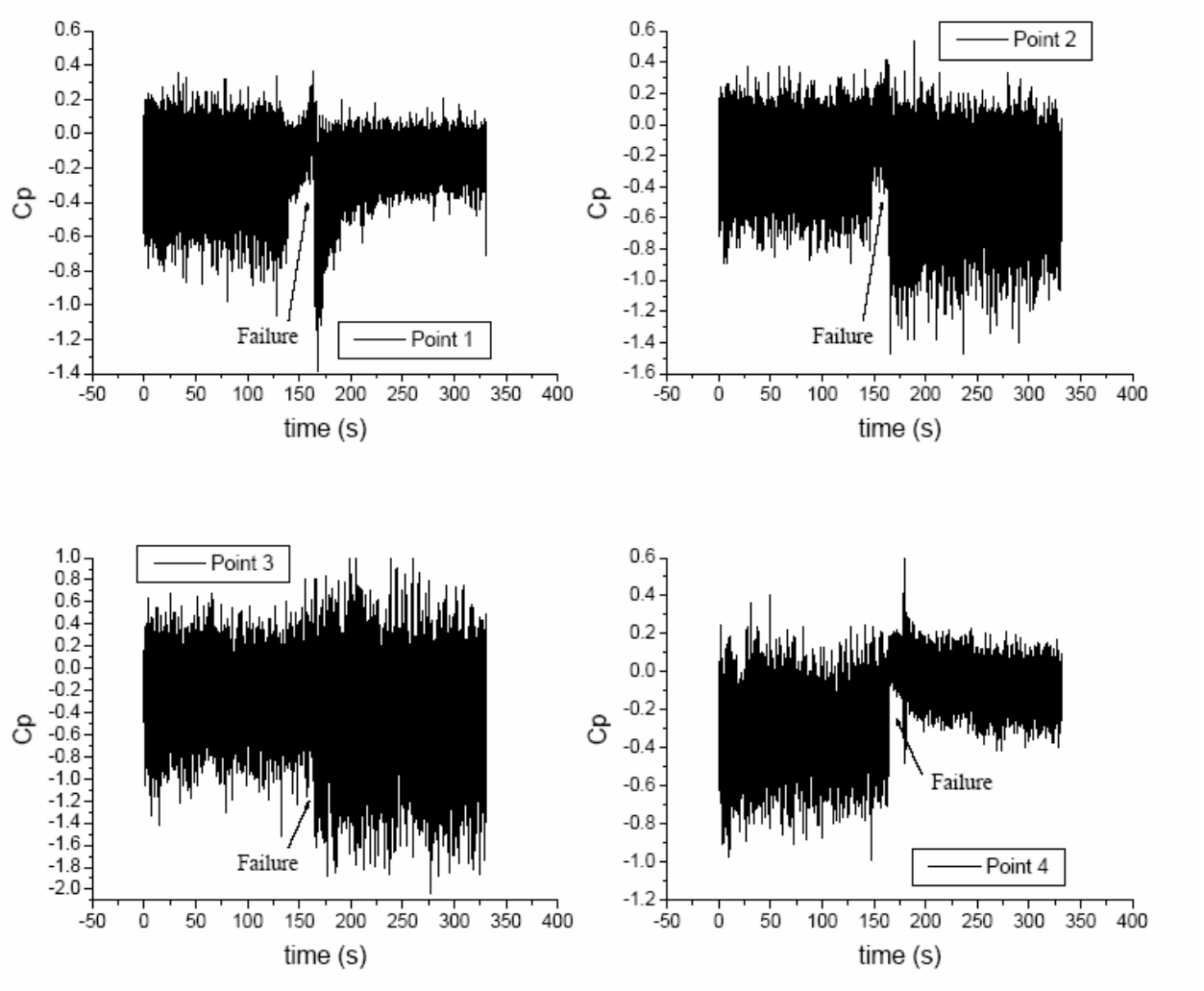

Figure 5.25: Pressure Time Histories for Model 2
(120 mph Wind Speed at 0° Direction)

5.3.4 Model 3 – Concrete Tiles with Foam

This roof system was first tested at 60 mph wind speed in the 50° direction for 6 minutes, with no damage observed. The 2-fan WoW was then oriented along the 0° angle, and the test procedure was repeated at 60 mph wind speed. No tile damage was visible at the end of this stage either. The wind speed was then increased to 120 mph, and was maintained for another 6 minutes. A few tiles at the windward edge failed followed by a series of tiles along the edge of the roof overhang (Figure 5.26).

The failure pattern of the roof tiles was observed to be the same as that of Models 1a, 1b, and 2, as shown in Figure 5.27. The pressure coefficients (C_{Pmean}, $C_{P\,RMS}$ and $C_{P\,\min}$) for each pressure tap at 60 mph wind speed in the 0° and 50° directions are listed in Tables 5.5 and 5.6, respectively. The pressure time histories of some typical positions (Points 2, 8, and 31) are shown in Figure 5.28.

(a) Roof Conditions Subjected to 120 mph Wind Speed at 50^{O} Direction

(b) Roof Conditions Subjected to 120 mph Wind Speed at 50^{O} Direction

Figure 5.26: Failure of Concrete-with-Foam Tile Roof System

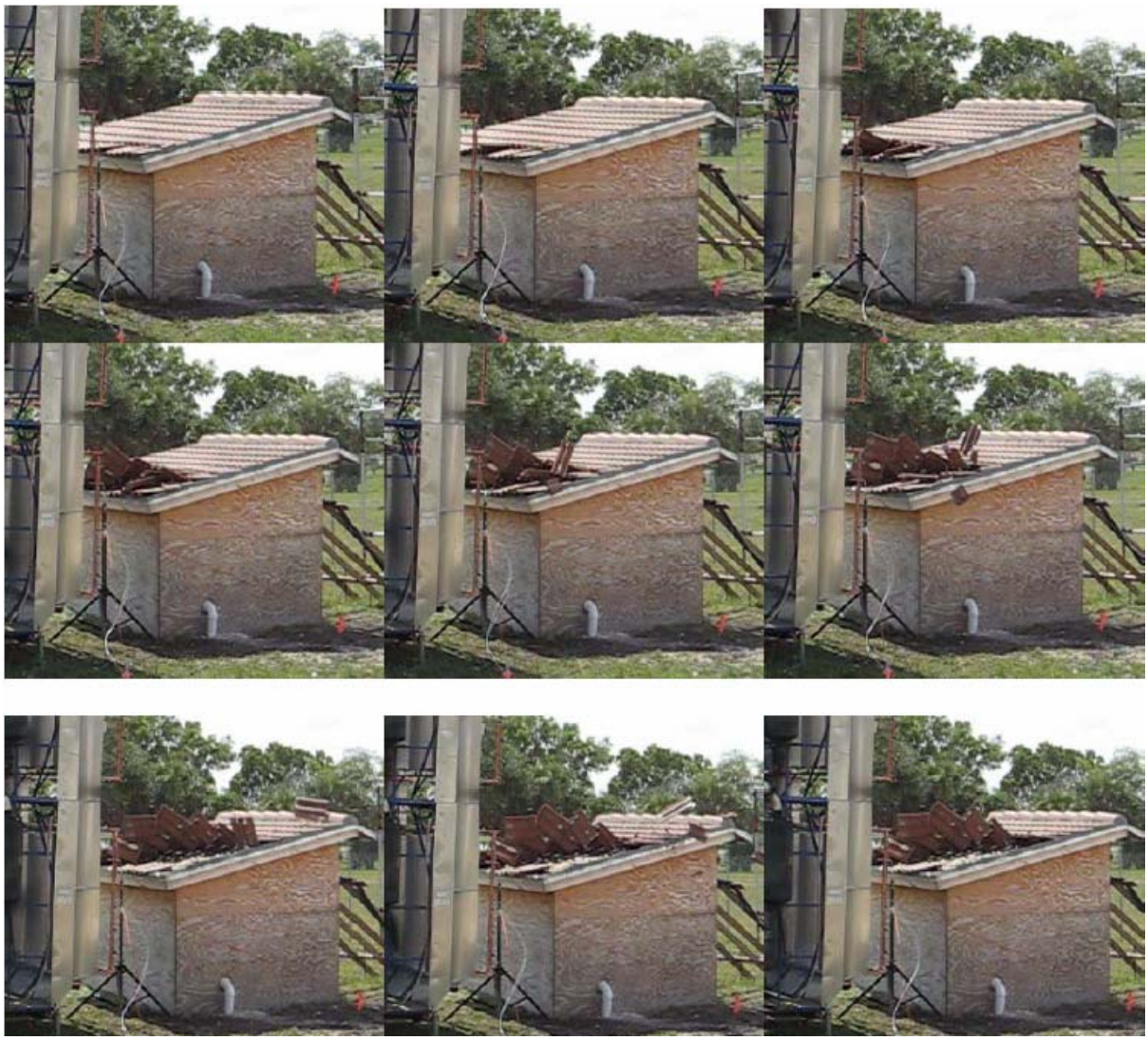

Figure 5.27: Failure Progress of Concrete-with-Foam Tile Roof System (120 mph Wind Speed at 0^o Direction)

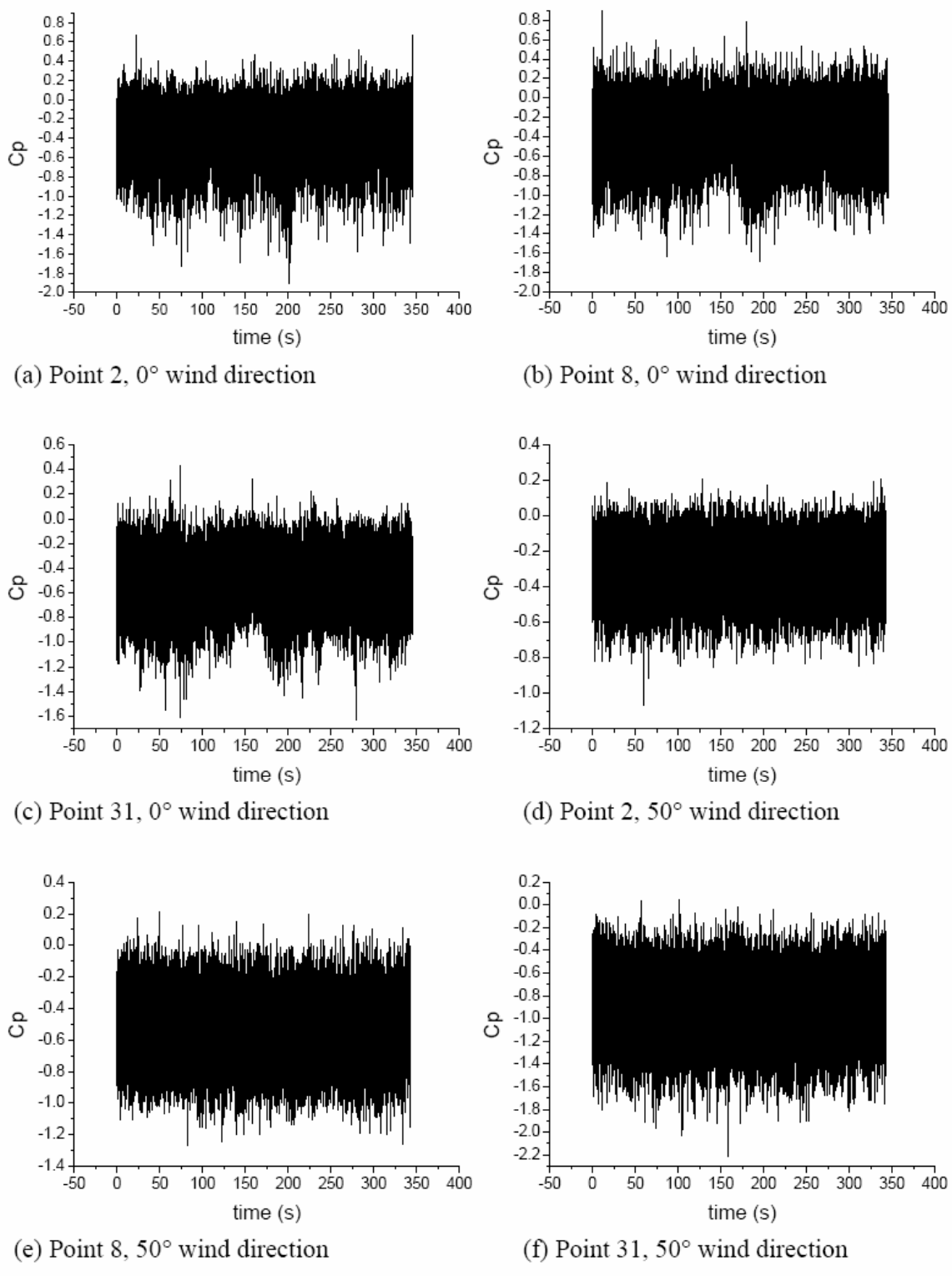

Figure 5.28: Pressure Time Histories for Model 3 (60 mph Wind Speed at 0^o and 50^o Directions)

5.3.5 Model 4 – Concrete Tiles with Mortar

This roof system was first tested at 60 mph wind speed in the 50° direction for 6 minutes, with no damage observed. The 2-fan WoW was then oriented along the 0^o angle and the test procedure was repeated at 60 mph wind speed. No tile damage was visible at the end of this stage either. The wind speed was then increased to 120 mph and was maintained at that speed for another 6 minutes. Again, no tiles were damaged or became visibly loose at the end of this test stage. The 2-fan WOW was then moved back to the 50^o wind direction position, and was run at 120 mph for another 6 minutes. All tiles remained firmly attached to the roof at the end of this test with no visible damage to any of the tiles. Figure 5.29 shows the model holding steady with no damage at the end of the test.

The pressure coefficients (C_{Pmean}, $C_{\mathrm{P}RMS}$ and $C_{P\min}$) for each pressure tap at 60 mph wind speed in the 0° and 50^o directions are listed in Tables 5.5 and 5.6, respectively. The pressure time histories of some typical positions (Points 2, 8, and 31) are shown in Figure 5.30.

Figure 5.29: Concrete-with-Mortar Tile Roof System after Wind Testing

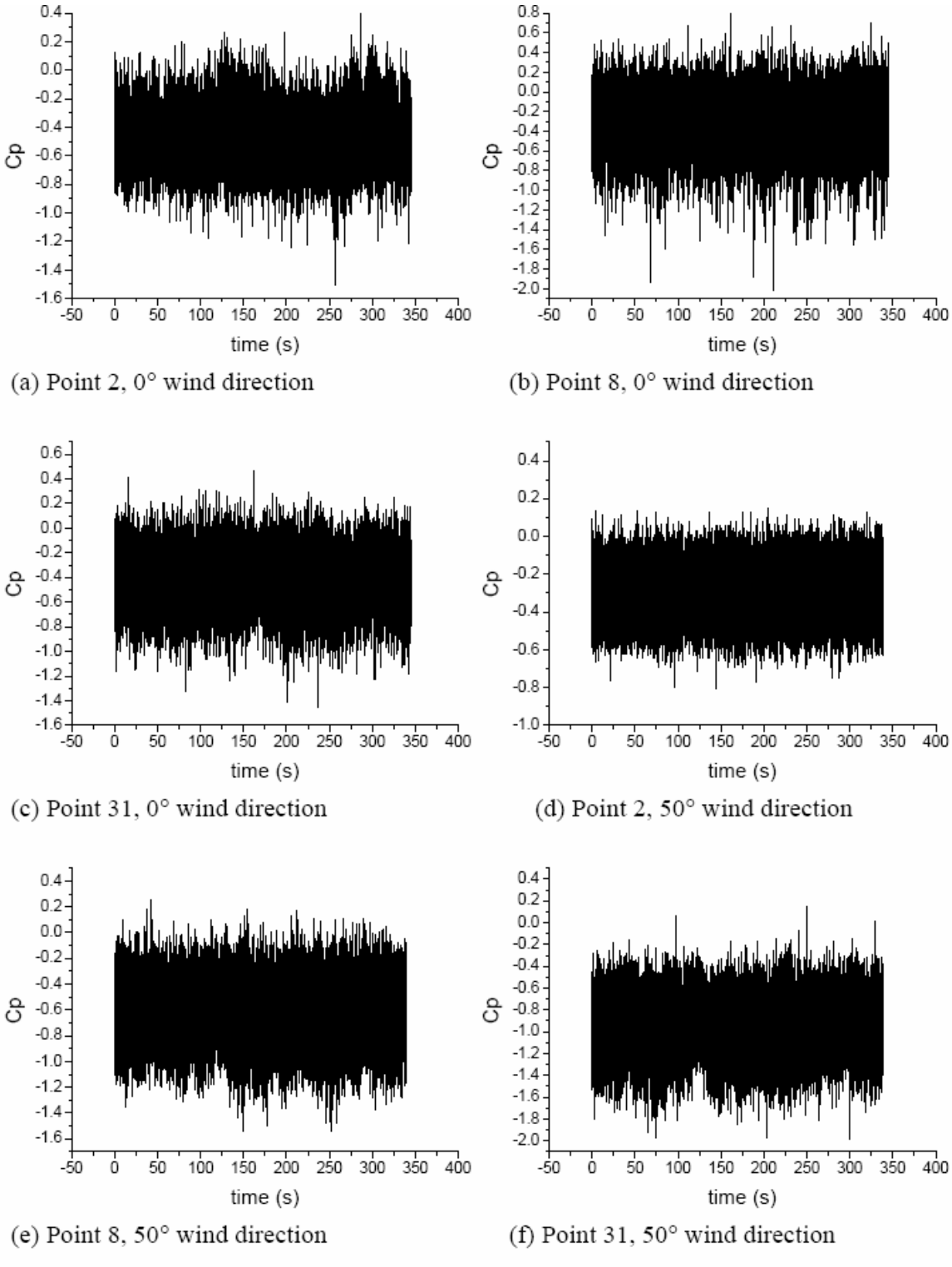

Figure 5.30: Pressure Time Histories for Model 4 (60 mph Wind Speed at 0^o and 50^o Directions)

Table 5.5: Pressure Coefficients (C_{Pmean}, $C_{P\,RMS}$ and $C_{P\min}$) of Concrete Tile Roofs (60 mph Wind Speed at 0° Direction)

Points	Model 3			Model 4		
	C_{Pmean}	$C_{P\,RMS}$	$C_{P\min}$	C_{Pmean}	$C_{P\,RMS}$	$C_{P\min}$
1	-0.39	0.21	-1.52	-0.52	0.18	-1.40
2	-0.34	0.25	-1.91	-0.47	0.17	-1.51
3	-0.17	0.28	-1.67	-0.23	0.17	-0.98
4	-0.50	0.23	-1.77	-0.44	0.17	-1.67
5	-0.37	0.17	-1.20	-0.19	0.14	-0.86
6	-0.26	0.20	-1.39	-0.10	0.19	-1.32
7	-0.13	0.32	-1.25	-0.15	0.36	-1.36
8	-0.33	0.26	-1.68	-0.27	0.24	-2.01
9	-0.39	0.13	-0.91	-0.43	0.13	-0.99
10	-0.20	0.12	-0.65	-0.19	0.12	-0.67
11	-0.09	0.13	-0.65	-0.14	0.12	-1.10
12	-0.18	0.14	-0.88	-0.09	0.12	-0.69
13	-0.29	0.21	-1.16	-0.19	0.21	-1.29
14	-0.26	0.12	-0.82	-0.26	0.11	-0.77
15	-0.29	0.12	-0.74	—	—	—
16	-0.22	0.14	-1.06	-0.14	0.15	-0.74
17	-0.03	0.17	-0.68	0.03	0.12	-0.49
18	-0.06	0.13	-0.61	0.12	0.44	-0.60
19	0.04	0.11	-0.39	-0.08	0.12	-0.51
20	-0.06	0.14	-0.70	-0.04	0.13	-0.61
21	0.07	0.12	-0.37	0.06	0.12	-0.38
22	-0.06	0.15	-0.68	-0.07	0.14	-0.66
23	-0.27	0.13	-0.84	-0.33	0.13	-0.84
24	-0.29	0.12	-0.80	-0.35	0.12	-0.82
25	-0.19	0.14	-0.76	-0.15	0.12	-0.58
26	-0.21	0.11	-0.88	-0.21	0.10	-0.65
27	-0.21	0.13	-0.78	-0.30	0.12	-0.80
28	-0.34	0.11	-0.90	-0.32	0.10	-0.69
29	0.10	0.14	-0.54	0.24	0.14	-0.35
30	-0.61	0.14	-1.16	-0.61	0.13	-1.14
31	-0.52	0.21	-1.62	-0.41	0.21	-1.46
32	0.48	0.13	-0.03	0.53	0.13	0.09

Table 5.6: Pressure Coefficients (C_{Pmean}, $C_{P\,RMS}$ and $C_{P\min}$) of Concrete Tile Roofs (60 mph Wind Speed at 50° Direction)

Points	Model 3			Model 4		
	C_{Pmean}	$C_{P\,RMS}$	$C_{P\min}$	C_{Pmean}	$C_{P\,RMS}$	$C_{P\min}$
1	-0.34	0.13	-0.87	-0.31	0.12	-0.77
2	-0.31	0.15	-1.07	-0.29	0.13	-0.81
3	-0.20	0.15	-0.95	0.00	0.14	-0.66
4	-0.45	0.18	-1.28	-0.32	0.13	-0.88
5	-0.28	0.24	-1.55	0.00	0.19	-0.73
6	-0.36	0.22	-1.39	-0.37	0.20	-1.24
7	-0.46	0.35	-1.71	-0.66	0.38	-1.99
8	-0.53	0.19	-1.27	-0.63	0.22	-1.54
9	-0.59	0.14	-1.19	-0.61	0.14	-1.18
10	-0.28	0.14	-0.89	-0.23	0.13	-0.75
11	-0.61	0.16	-1.30	-0.35	0.17	-1.23
12	-0.66	0.21	-1.74	-0.48	0.15	-1.26
13	-0.84	0.27	-2.11	-0.63	0.23	-1.48
14	-0.47	0.14	-1.10	-0.43	0.14	-0.96
15	-0.27	0.15	-0.82	—	—	—
16	-0.71	0.21	-1.68	-0.51	0.18	-1.96
17	-0.15	0.18	-0.88	-0.07	0.13	-0.63
18	-0.46	0.18	-1.43	-0.26	0.70	-1.22
19	-0.05	0.12	-0.54	-0.16	0.13	-0.83
20	-0.47	0.20	-1.49	-0.33	0.17	-1.14
21	-0.05	0.13	-0.59	-0.03	0.13	-0.55
22	-0.27	0.18	-1.32	-0.13	0.16	-1.00
23	0.00	0.15	-0.58	-0.12	0.14	-0.75
24	-0.26	0.12	-1.14	-0.29	0.18	-1.12
25	0.00	0.15	-0.61	0.03	0.12	-0.43
26	-0.28	0.14	-0.94	-0.37	0.13	-1.06
27	-0.42	0.16	-1.20	-0.42	0.16	-1.15
28	-0.34	0.14	-1.08	-0.40	0.13	-1.15
29	0.13	0.14	-0.36	0.13	0.14	-0.49
30	-0.65	0.18	-1.46	-0.73	0.18	-1.61
31	-0.87	0.27	-2.22	-0.94	0.24	-1.99
32	0.44	0.12	-0.06	0.47	0.12	0.01

5.4 Discussion of WoW Test Results

The test results presented above show that the tiles along the roof eave experience the maximum wind force and therefore are most susceptible to fail first. The test results also show that the failure of these tiles may result in the failure of the remaining roof tiles in a domino pattern (see Figures 5.16, 5.19, 5.23 and 5.27). This domino pattern of failure is

due to two main reasons: the interaction between the joined tiles; and the fact that the tiles become compromised once one tile is blown off and wind starts to flow under the remaining tiles. These observations suggest reinforcing the connection between the eave tiles and the roof board to better resist the hurricane impact.

In Model 1b (clay tiles roof with foam), the roof tiles held on for about $3^{1/2}$ minutes at 120 mph wind speed, while the same type of roof tiles in Model 1a (clay tiles roof with foam) failed almost instantaneously at 120 mph wind speed. One of the main reasons for the observed difference is roofer's workmanship. The two roof structures were built by two different contractors, and the quantity of adhesive applied by each contractor was different. According to site measurements after wind tests, the average contact area of the foam between the clay tiles and the roof board in Model 1a was 4.7 in. × 2.5 in. (average of 10 samples), while the corresponding value was 6 in. × 2.5 in. in Model 1b, or approximately 28% more than that in Model 1a.

It is evident that the amount of connecting materials (foam and mortar) used by contractors in the WoW tests were much less than those used in the mechanical uplift laboratory tests (compare for example, Figure 5.31 with Figures 3.16−3.19). Therefore, it appears that poor workmanship and lack of adherence to the code, are the two main contributing factors to premature failure of tile roofs.

5.5 Comparison of WoW Test Results with ASCE 7-05

5.5.1 Mean Pressure Coefficients

The distribution of the mean pressure coefficients in the five tests described in Section 5.4 shows a similar trend. In the 0° wind direction, the absolute values of the pressure coefficients on the windward roof edge are the largest. Along the wind direction, the suction is reduced to the point where at times it may become positive pressure on the middle of the roof. Close to the ridge, the absolute value of negative pressures increases gradually. For the ridge tiles, there are positive pressures on the windward surfaces and suctions on the top and leeward surfaces.

The external pressure coefficients, C_p, for the main wind force resisting system (MWFRS) are specified in Figure 6-6 of ASCE 7-05. For this project; the roof angle θ is 18.4°; and h (mean roof height) / L (horizontal dimension of building) is 0.81 [(5.92+0.5×2.67) / 9].

According to the ASCE 7-05, C_p should be about -0.7. None of the mean pressure coefficients C_{Pmean} listed in Tables 5.3 and 5.5 in the 0° wind direction exceeded the code value.

(a) Clay Tile Roof with Foam in Model 1a

(b) Clay Tile Roof with Mortar in Model 2

Figure 5.31: Failure of Roof Tiles

5.5.2 Components and Cladding

In ASCE 7-05, the design wind pressures for components and cladding (Method 2) are calculated as follows:

$$q = 0.00256 \times K_z \times K_{zt} \times K_d \times I \times V^2 \quad (5.5)$$

where q is wind pressure; K_z is exposure factor; K_{zt} is topographic factor; K_d is directionality factor; I is importance factor; and V is the basic design wind speed corresponding to a 3-second gust at 33 ft above ground in exposure Category C.

$$p_s = q \times [(GC_p) - (GC_{pi})] \quad (5.6)$$

where p_s is the net design wind pressure; GC_p is the external pressure coefficient; and GC_{pi} is the internal pressure coefficient.

The tile roof test structure used in this experimental work is considered by the ASCE 7-05 Specifications to be a partially enclosed building with a monoslope roof. Accordingly, GC_p varies depending on the zone for which the pressure is calculated, as listed in Table 5.7 and shown in Figure 5.32.

Table 5.7: Value of GCp for Monoslope Roofs ($10° < \theta \leq 30°$) in ASCE 7-05

Design Zone	Suction			Positive Pressure
	Zone 1	Zone 2	Zone 3	Zone 1, 2 and 3
GCp	-1.3	-1.6	-2.9	+0.4

Note: Effective wind area is selected to be less than 10 ft^2, and a is 3 ft.

Below, the minimum pressure coefficients (C_{pmin}) on the roof tiles of the WoW experiments are compared with the external pressure coefficient GC_p in ASCE 7-05.

For Zone 1, only Point 21 in the clay tile roof was located in this area (see Figure 5.32). The lowest C_{pmin} was recorded to be -0.84 (Model 2, 0° wind direction), with an absolute value less than that specified by ASCE 7-05. In the concrete tile roofs, Points 17 and 19 were located in this area. The lowest C_{pmin} was recorded to be -0.88 (Point 17, Model 3, 50° wind direction), with an absolute value again less than that specified by ASCE 7-05.

For Zone 2, the C_{pmin} coefficients recorded in the WoW testing far exceeded the design values in ASCE 7-05. The largest C_{pmin} (absolute value) in the clay tile roofs, -3.74, occurred at Point 10 (Model 1b, 50° wind direction), which is about 2.33 times the GCp (-1.6) specified by ASCE 7-05. For the concrete tile roofs, the largest $C_{pmin,}$ -2.11, occurred at Point 13 (Model 3, 50° wind direction), which is about 1.32 times the GC_p (-1.6) specified by ASCE 7-05.

For Zone 3, the code provides the largest GC_p as -2.9, whereas in the WoW test for clay tile roofs, the largest C_{pmin} of Points 24−32 was only -2.00 (Model 1a, Point 31, 0° wind

direction). For the concrete tile roofs, the largest C_{pmin} of Points 21−32 was only -2.22 (Model 3, Point 31, 50° wind direction). This may be attributed mainly to the fact that the code considers an aggregate of all wind directions (i.e., 0°−360°), while this monoslope structure was subject only to the 0° and 50° wind directions in the WoW testing.

This comparison suggests that the ASCE 7-05 values should be re-evaluated, as they may not be conservative, specifically at the corners of the roofs.

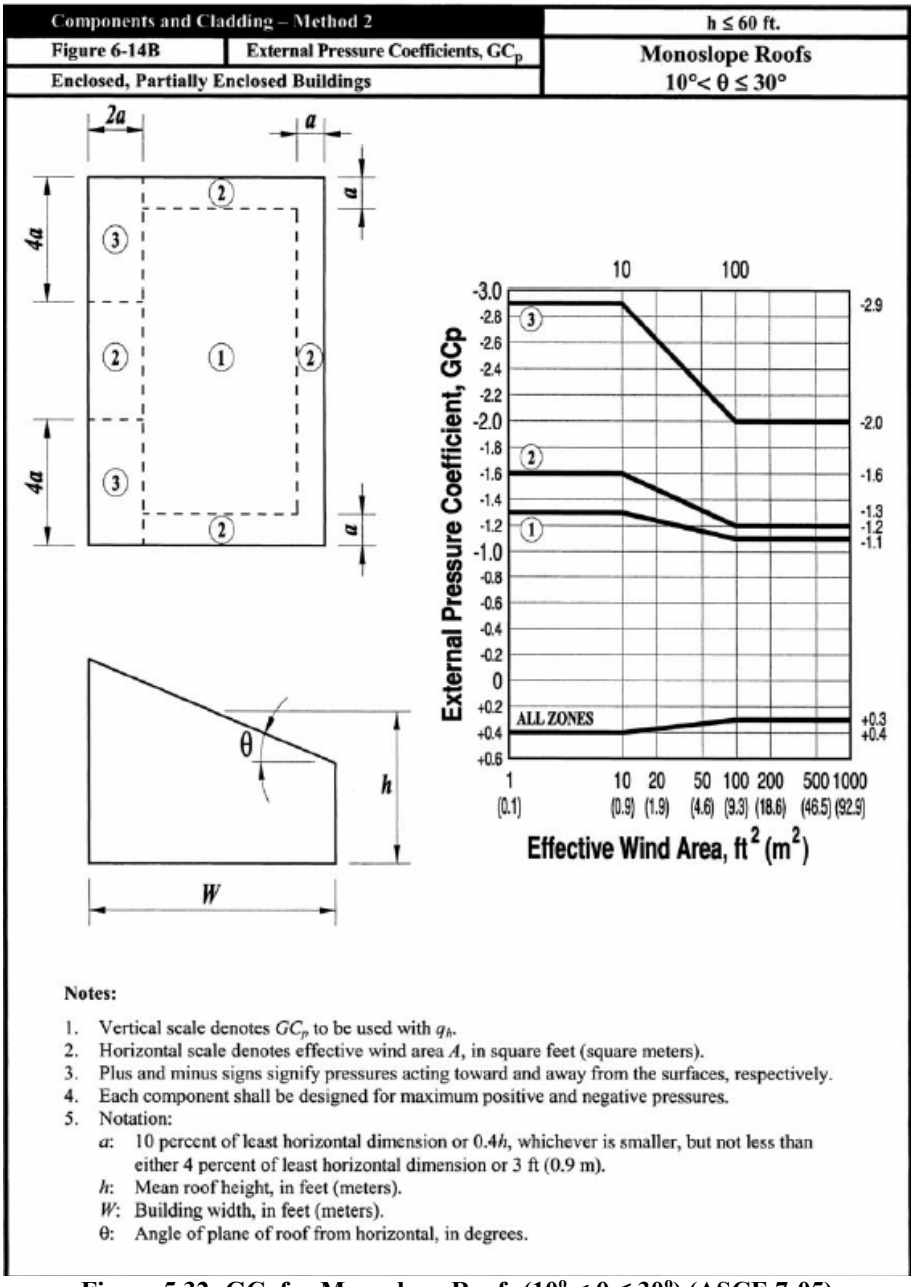

Figure 5.32: GC_p for Monoslope Roofs ($10^o < \theta \leq 30^o$) (ASCE 7-05)

6.0 Finite Element Analysis

The data obtained from the mechanical uplift testing was used to first develop a finite element model for a single ridge or field (clay or concrete) tile. The model was then expanded to the entire roof system, consisting of the field and ridge tiles, the backing materials, the roof deck, and the roof truss. The general purpose software, ANSYS Version 8.0 was used for the finite element modeling (FEM) of tile roof system. The analysis results were then compared with the wind loads obtained during the Wall Wind (WoW) testing. The model developed in this study can be used for further analysis of various tile roof systems under dynamic and impact loading.

6.1 Material Modeling of Clay and Concrete Tiles

Elastic (Young's) modulus of the tiles is an important material property in their FEM simulation. Therefore, coupon tests of clay and concrete tiles were carried out in the laboratory in accordance with ASTM Standard E111-04, *Standard Test Method for Young's Modulus, Tangent Modulus, and Chord Modulus*, which covers procedures to determine the elastic modulus of concrete and clay tiles.

Figure 6.1 shows a strip of a clay tile under axial compression in the lab, with a mounted strain gage. The elastic modulus (E_x) can be calculated, as

$$E_x = \frac{\sigma}{\varepsilon} = \frac{P/A}{\varepsilon} \tag{6.1}$$

where P is the axial compressive force, A is the cross-sectional area of the strip of tile, and ε is the axial strain measured on the tile. Figure 6.2 shows the measured axial stress-strain response curve for two samples of clay tile, leading to an average elastic modulus of 2×10^6 psi for clay tiles. Similar tests on samples of concrete tiles led to an average elastic modulus of 3×10^6 psi for concrete tiles (see Figures 6.3 and 6.4).

6.2 Modeling of Single Ridge and Field Tiles

The clay and concrete tiles, as well as the plywood deck, were discretized using elastic shell (Shell63) elements. The truss members were modeled using three-dimensional beam (Beam4) elements. The interface between the roof tiles and the plywood deck, i.e., the foam or mortar, poses the most challenging issues for finite element modeling. In this study, the attachment interface was modeled using nonlinear spring (Combin39) elements. The mechanical uplift test data were used to calibrate the spring constants for the interface elements. Table 6.1 shows the material properties for the various components of the roof system. For accurate modeling of single tiles, a series of laboratory experiments were carried out, as described in the following sections.

Figure 6.1: Clay Tile Strip under Axial Compression

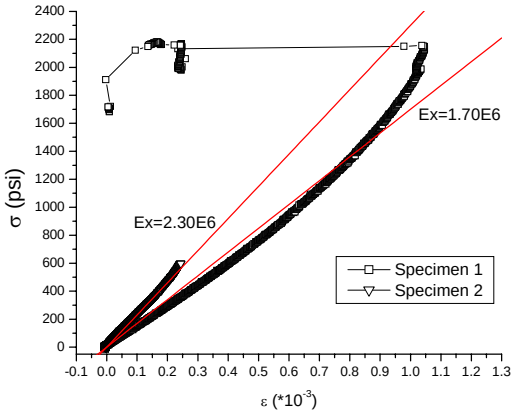

Figure 6.2: Axial Stress-Strain Response of Clay Tiles

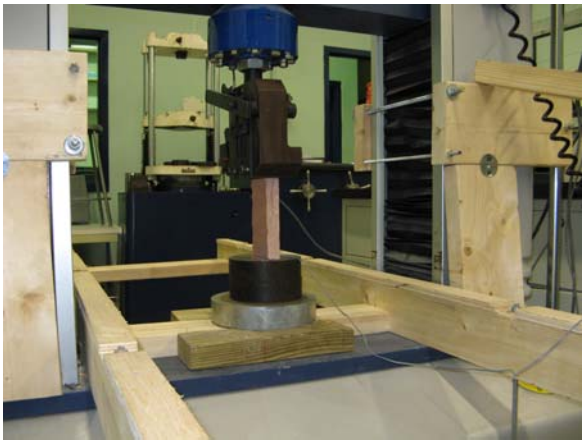

Figure 6.3: Concrete Tile Strip under Axial Compression

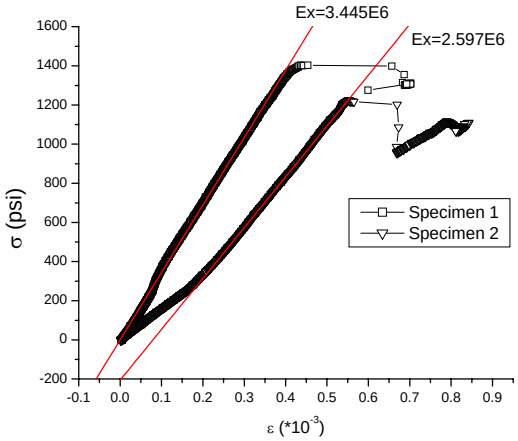

Figure 6.4: Axial Stress-Strain Response of Concrete Tiles

Table 6.1: Material Properties of Various Components of the Roof System

	Clay Tile	Concrete Tile	Timber
Elastic Modulus (psi)	2.0×10^6	3.0×10^6	$1.2 \times 10^{6*}$
Poisson's Ratio	0.20	0.20	0.29
Mass Density (lb/in^3)	0.05	0.05	0.02
Thickness (in.)	½	½	½

* Average of the range ($0.9 - 1.6 \times 10^6$ psi) given by *National Design Specifications for Wood Construction* (American Society of Agricultural and Biological Engineers, 2001)

6.2.1 Single Ridge Tile with Adhesive-Set

Similar to the mechanical uplift tests described in Section 3, single clay and concrete ridge tiles with adhesive-set were attached to a 2"x 6" wood member that was in turn mechanically fastened to the roof deck, as shown in Figure 6.5. The figure shows the positions of potentiometers (Points A, E, and F) where the displacements of the system were measured using a high-speed data acquisition system. Figure 6.6 shows the load-deflection curves for the clay and concrete ridge tiles with adhesive-set (foam). The

stiffness of the interface was then calculated based on the difference of the load-deflection response at the center point of the tile (Point A) and the average of the responses at the edges of the tile (Points E and F). Figure 6.7 shows the constructed load-deflection curve for the interface adhesive.

The ridge tile was meshed using 216 shell elements with 18 and 12 equal divisions in the longitudinal and transverse directions, respectively. All elements were restrained along the longitudinal axis, and the plywood board was affixed at the corners using pin supports. The load was applied at the center of the tile to simulate the mechanical uplift tests. The ANSYS model of the single ridge tile system is shown in Figure 6.8. Nonlinear spring parameters used in the model are shown in Figure 6.9. Comparison of the ANSYS model simulation and the test results indicate good agreement, as shown in Figure 6.10.

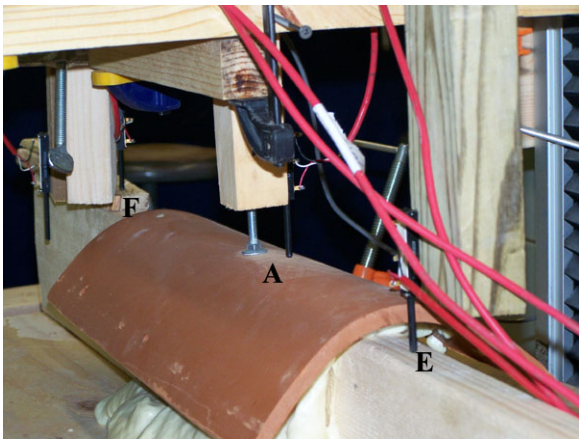

Figure 6.5: Ridge Tile Test with Adhesive-Set and Potentiometers at Points A, E, and F

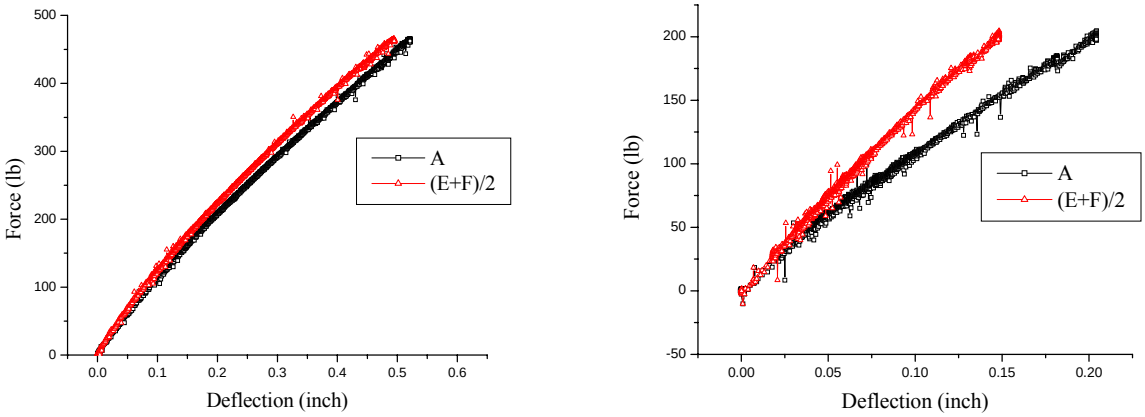

(a) Clay Ridge Tile (b) Concrete Ridge Tile

Figure 6.6: Load-Deflection Curves of Ridge Tile with Adhesive-Set

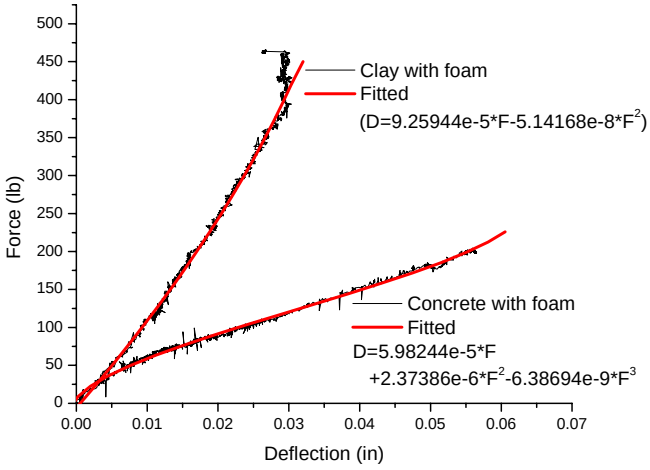

Figure 6.7: Constructed Load-Deflection of the Adhesive Interface

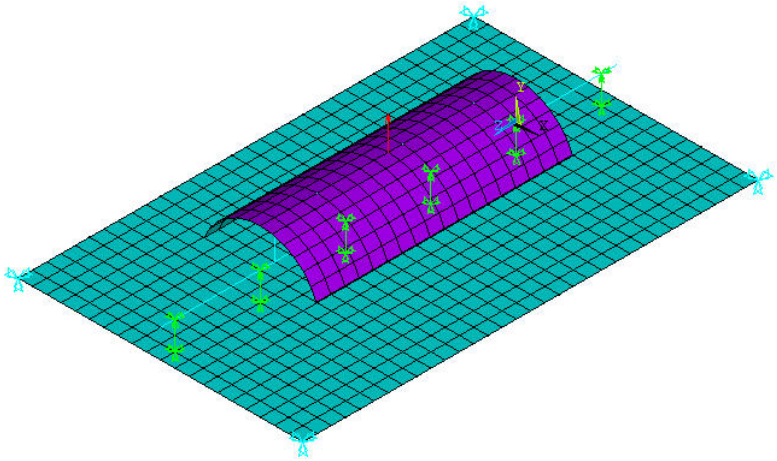

Figure 6.8: ANSYS Model of Single Ridge Tile System

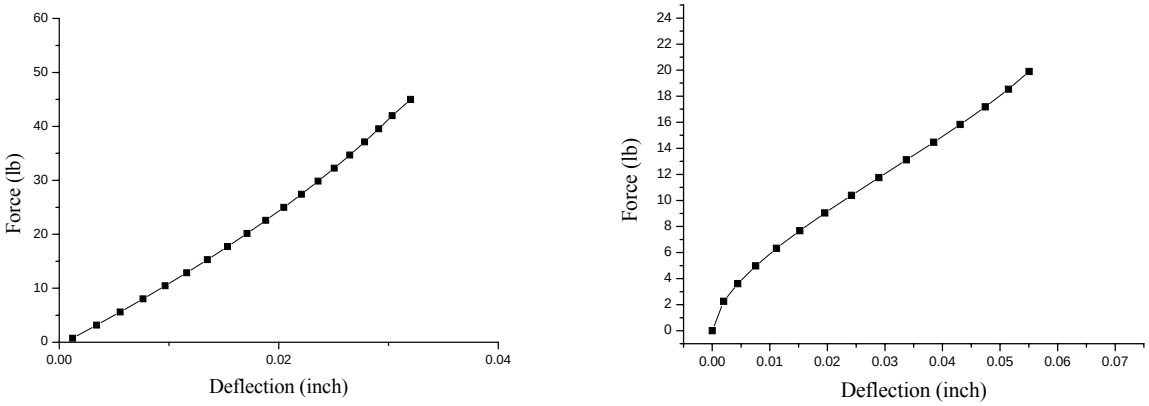

(a) Clay Ridge Tile with 10 Springs (b) Concrete Ridge Tile with 10 Springs

Figure 6.9: Nonlinear Spring Parameters Used in ANSYS Model for Adhesive-Set

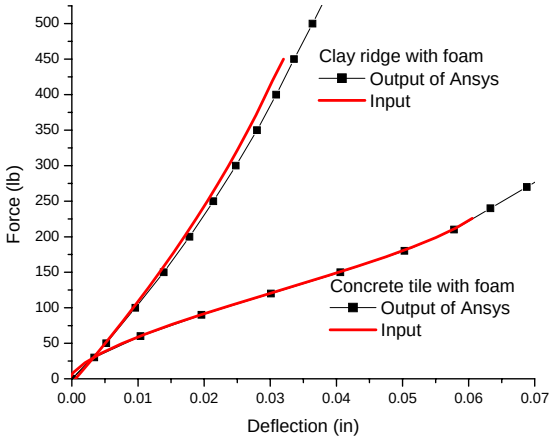

Figure 6.10: Comparison of ANSYS Simulation and Test Data for Adhesive-Set Interface

6.2.2 Single Ridge Tile with Mortar-Set

Figure 6.11 shows the test set up for ridge tiles with mortar-set placed on three field tiles that were in turn mechanically attached to the ½" plywood deck, as described in Section 3. The figure shows the positions of potentiometers (Points A-D), where the displacements of the system were measured. Figure 6.12 shows the load-deflection of clay and concrete ridge tiles with mortar-set. The stiffness of the interface was then calculated based on the measurements of the potentiometers, similar to the procedure described for the adhesive-set. Figure 6.13 shows the constructed load-deflection curve for the interface mortar. The finite element mesh was similar to that described for the adhesive-set. Comparison of the simulation and test results of the interface are shown in Figure 6.14, which confirms good agreement.

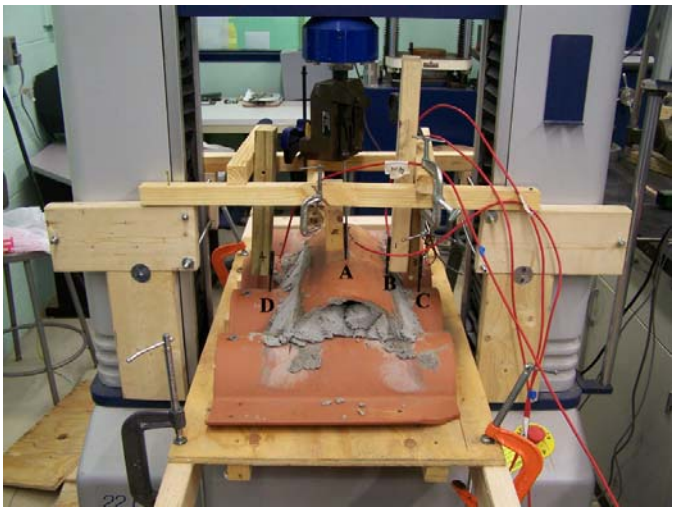

Figure 6.11: Ridge Tile Test with Mortar-Set and Potentiometers at Points A-D

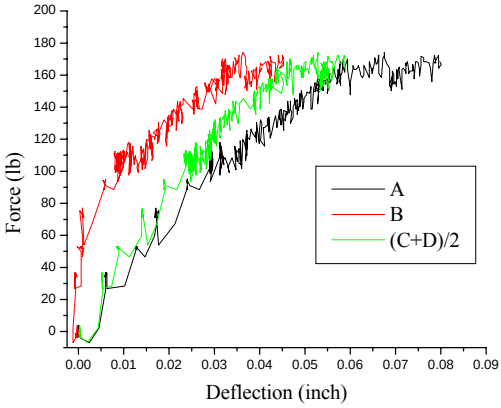

(a) Clay Ridge Tile

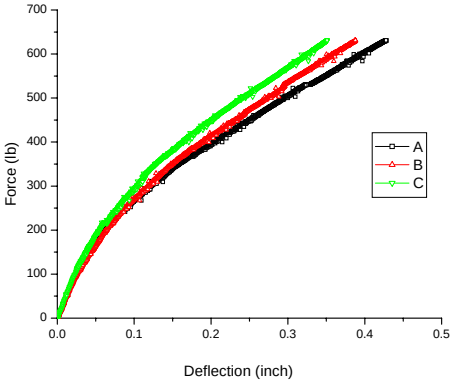

(b) Concrete Ridge Tile

Figure 6.12: Load-Deflection Curves of Ridge Tile with Mortar-Set

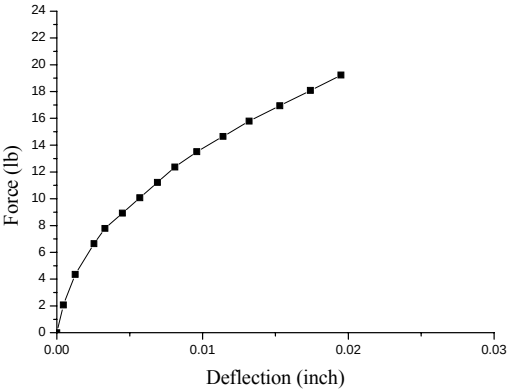

(a) Clay Ridge Tile with 10 Springs

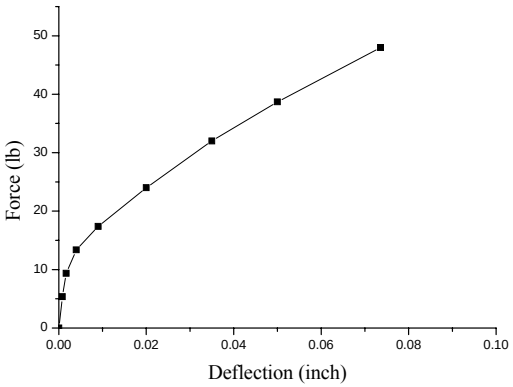

(b) Concrete Ridge Tile with 10 Springs

Figure 6.13: Nonlinear Spring Parameters Used in ANSYS Model for Mortar-Set

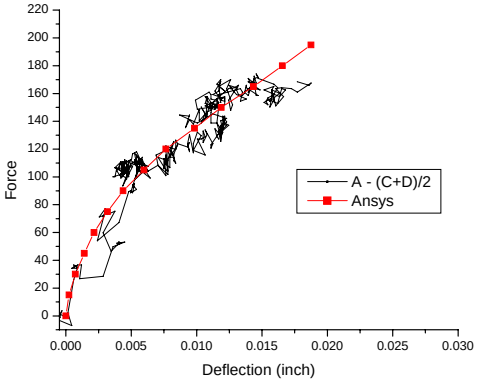

(a) Clay Ridge Tile

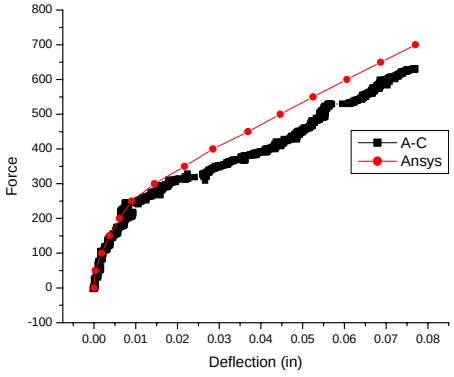

(b) Concrete Ridge Tile

Figure 6.14: Comparison of ANSYS Simulation and Test Data for Mortar-Set Interface

6.2.3 Single Field Tile with Adhesive-Set

The single clay or concrete field tile was attached with adhesive-set (foam) to a hot mopped 30/90 deck underlayment, and a ½" plywood decking, as described in Section 3. Figure 6.15 shows the locations of potentiometers (Points 1-4), where displacements of the system were measured. The clay field tile was meshed using 288 elements with 18 and 16 equal divisions in the longitudinal and transverse direction, respectively. The concrete field tile was meshed using 378 elements with 18 and 21 equal divisions in the longitudinal and transverse direction, respectively. The plywood board was affixed at the corners using pin supports. The ANSYS models for the clay and concrete field tiles are shown in Figure 6.16.

The constants for the springs at the adhesive interface were calibrated using the load-deflection test data, shown in Figure 6.17, leading to the nonlinear spring parameters shown in Figure 6.18.

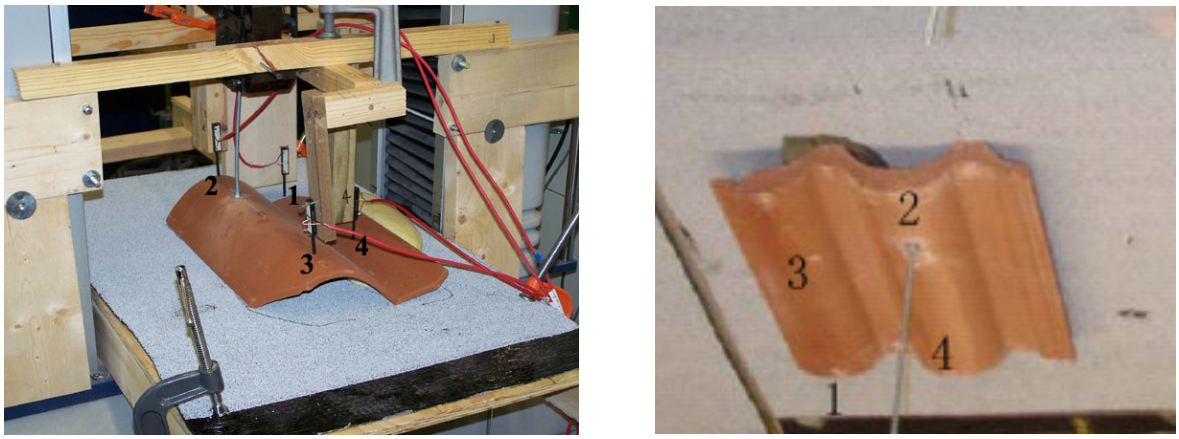

(a) Clay Field Tile (b) Concrete Field Tile

Figure 6.15: Field Tile Test with Adhesive-Set and Potentiometers at Points 1-4

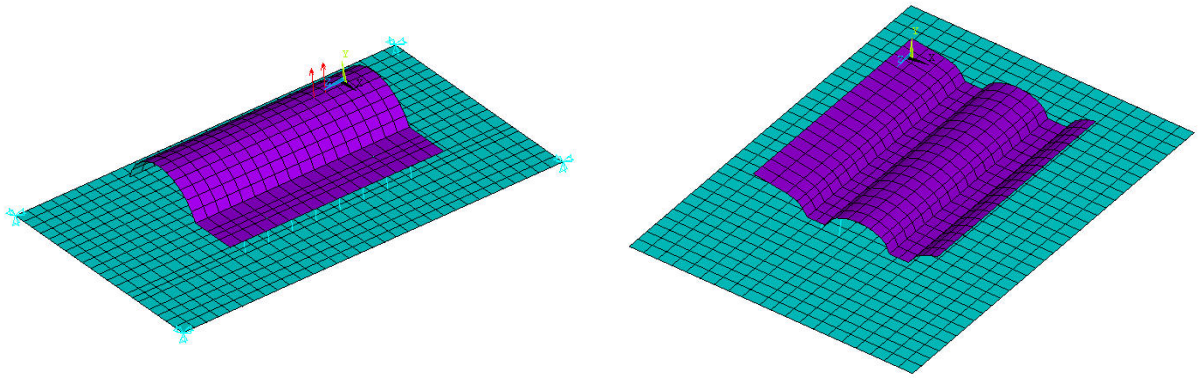

(a) Clay Field Tile (b) Concrete Field Tile

Figure 6.16: ANSYS Model of Single Field Tile System

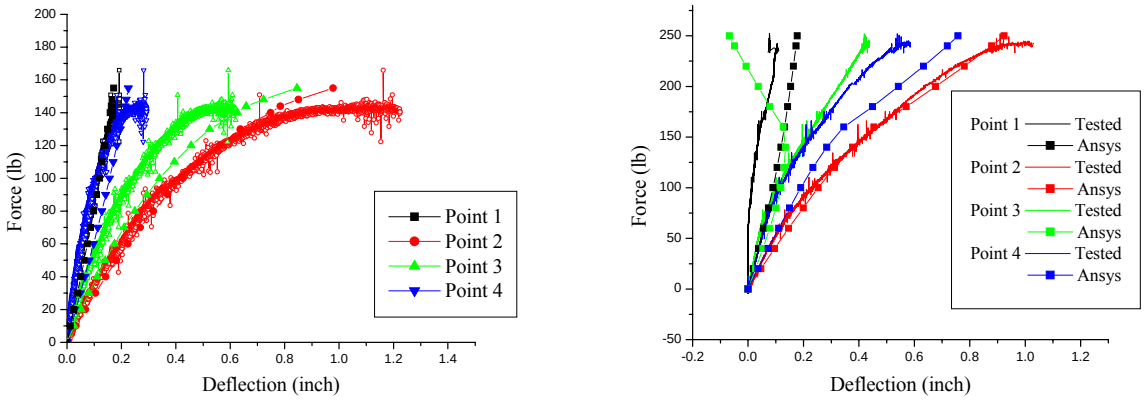

(a) Clay Field Tile (b) Concrete Field Tile

Figure 6.17: Comparison of ANSYS Simulation and Test Data for Adhesive-Set Interface

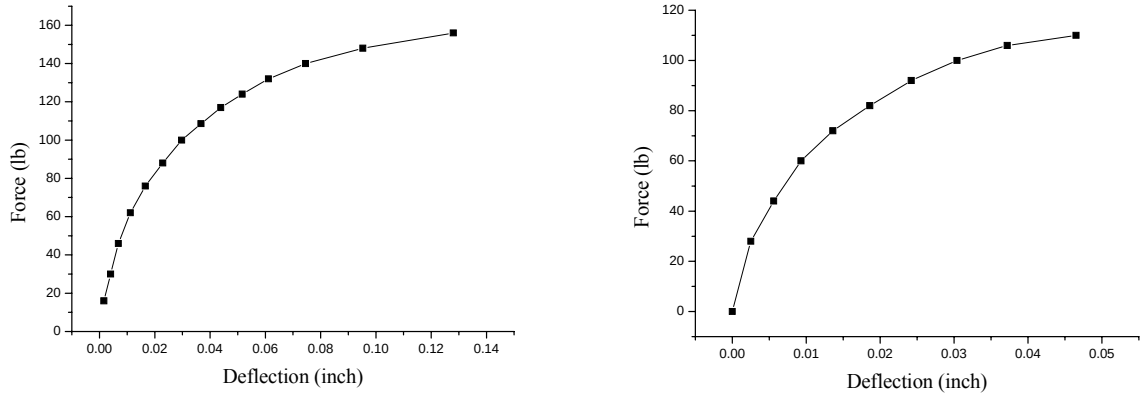

(a) Clay Field Tile with 8 Springs (b) Concrete Field Tile with 8 Springs

Figure 6.18: Nonlinear Spring Parameters Used in ANSYS Model

6.2.4 Single Field Tile with Mortar-Set

Figure 6.19 shows the locations of potentiometers (Points 1-4), where displacements of the system were measured. The meshing followed the same pattern as that described for the adhesive-set. Comparison of the simulation and test results of the interface are shown in Figure 6.20. The nonlinear spring parameters used in the ANSYS model are shown in Figure 6.21.

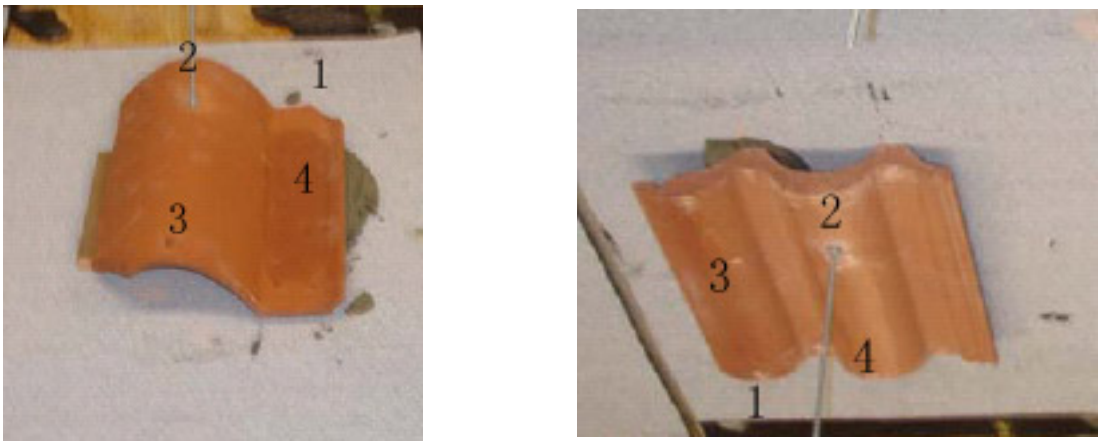

(a) Clay Field Tile (b) Concrete Field Tile

Figure 6.19: Field Tile Test with Mortar-Set and Potentiometer Positions at Points 1-4

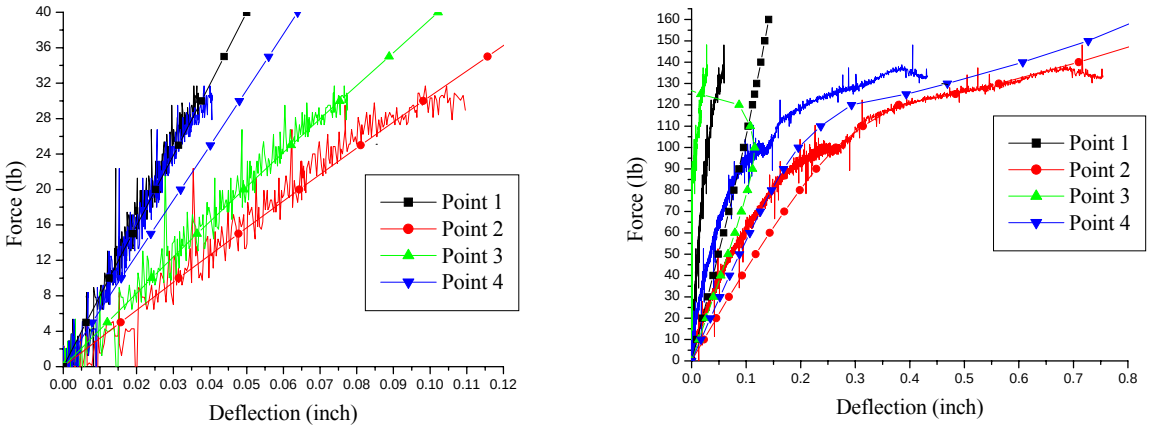

(a) Clay Field Tile (b) Concrete Field Tile

Figure 6.20: Comparison of ANSYS Simulation and Test Data for Mortar-Set Interface

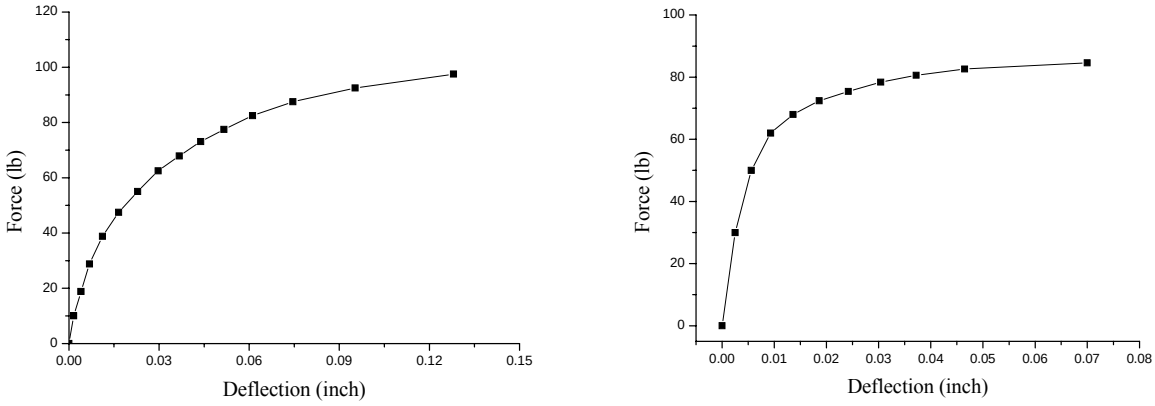

(a) Clay Field Tile with 8 Springs (b) Concrete Field Tile with 8 Springs

Figure 6.21: Nonlinear Spring Parameters Used in ANSYS Model

6.3 Simulation of Tile Roof System

Based on the calibration data of single ridge and field (clay and concrete) tiles obtained in Section 6.2, the finite element model for a large section of the roof system was assembled to simulate the effects of wind loads and to compare the results with the Wall of Wind (WoW) test data. The complete roof model consisted of field and ridge tiles, backing materials, roof deck, and the roof truss. The interaction between the tiles was also simulated in the model.

6.3.1 Wind Loads

As described in Section 5, wind pressures on tile roofs were measured using transducers in the Wall of Wind experiments. Because the roofs were mainly affected by the suction, the minimum pressure coefficients ($C_{P\min}$) were used to calculate the wind loads on tiles. For the ridge tile, the most severe loading case would occur when the windward surface is under positive pressure and the leeward surface is under negative pressure (suction). Therefore, the maximum pressure coefficients were used to calculate the wind pressure on the windward surface of the ridge tiles. The wind loads on each tile were calculated, as

$$F = 0.00256 * V^2 * C_{P\min} * A \tag{6.2}$$

where F is the wind load (lbs); V is the wind speed (mph); and A is the projected area in the direction of the wind force. Linear interpolation and symmetry were used to estimate wind pressure pattern on the entire roof based on the measured data of the pressure transducers. The minimum pressure coefficients on entire tile roofs used in the FEM analysis are shown in Figures 6.22-6.25.

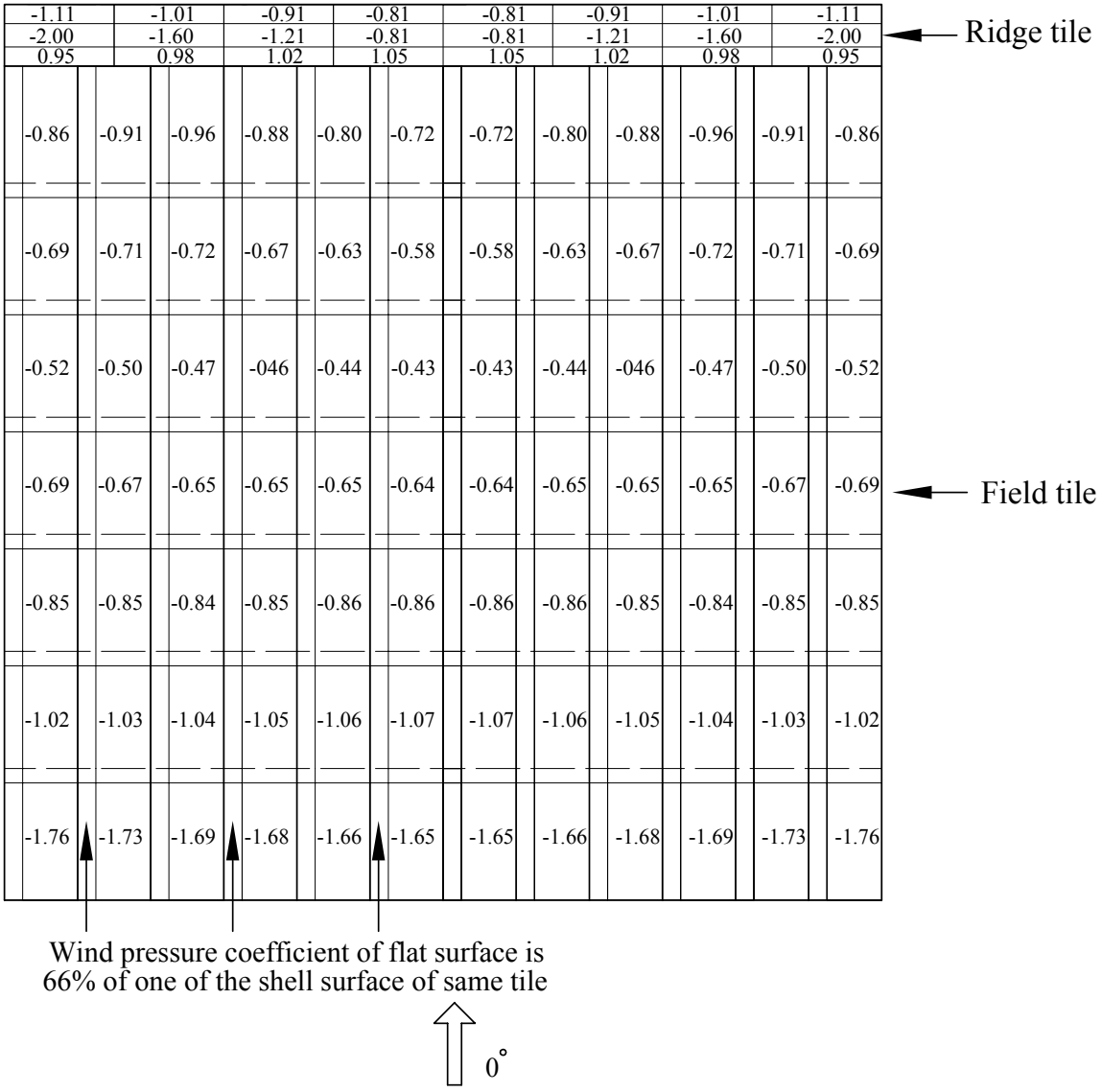

Notes:

1. The pressure coefficients were averaged from test data of Models 1a and 1b.
2. The wind pressure coefficient of flat portion of clay field tile was approximately 66% of that on the rounded surface of the tile.

Figure 6.22: Pressure Coefficients of Clay Tile Roof with Adhesive-Set Used in FEM

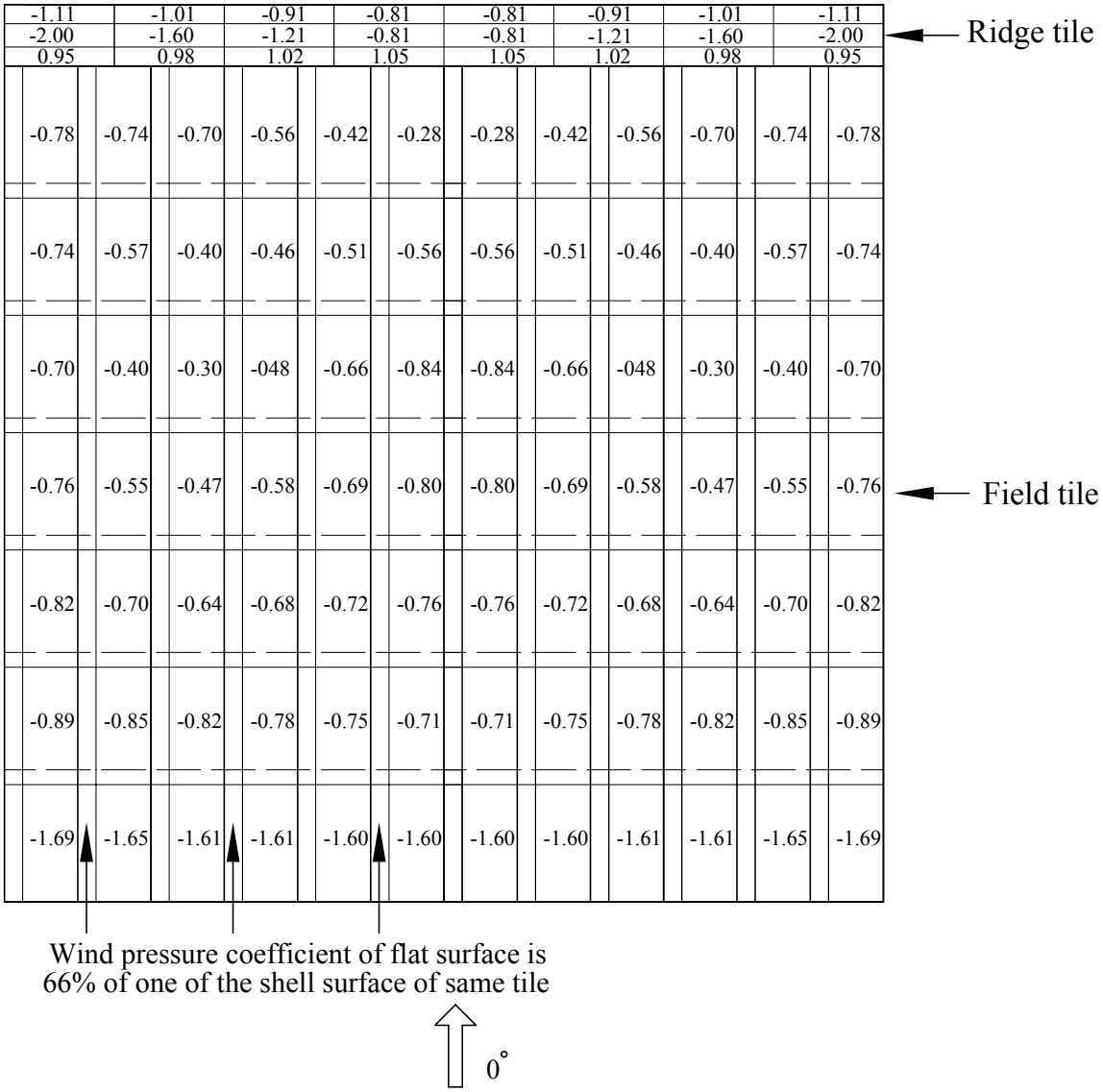

Note: The wind pressure coefficient of flat portion of clay field tile was approximately 66% of that on the rounded surface of the tile.

Figure 6.23: Pressure Coefficients of Clay Tile Roof with Mortar-Set Used in FEM

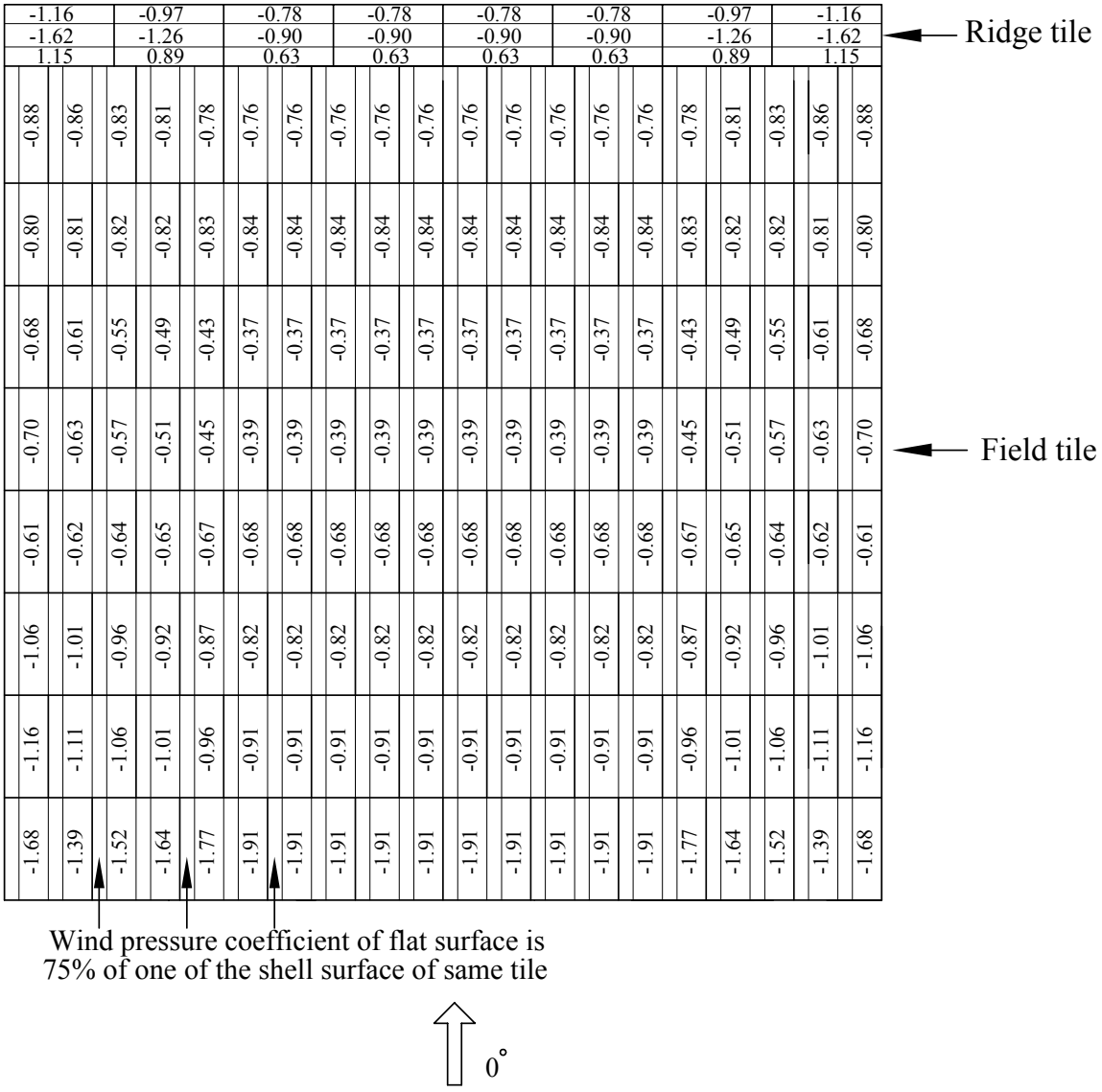

Note: The wind pressure coefficient of flat portion of concrete field tile was approximately 75% of that on the rounded surface of the tile.

Figure 6.24: Pressure Coefficients of Concrete Tile Roof with Adhesive-Set Used in FEM

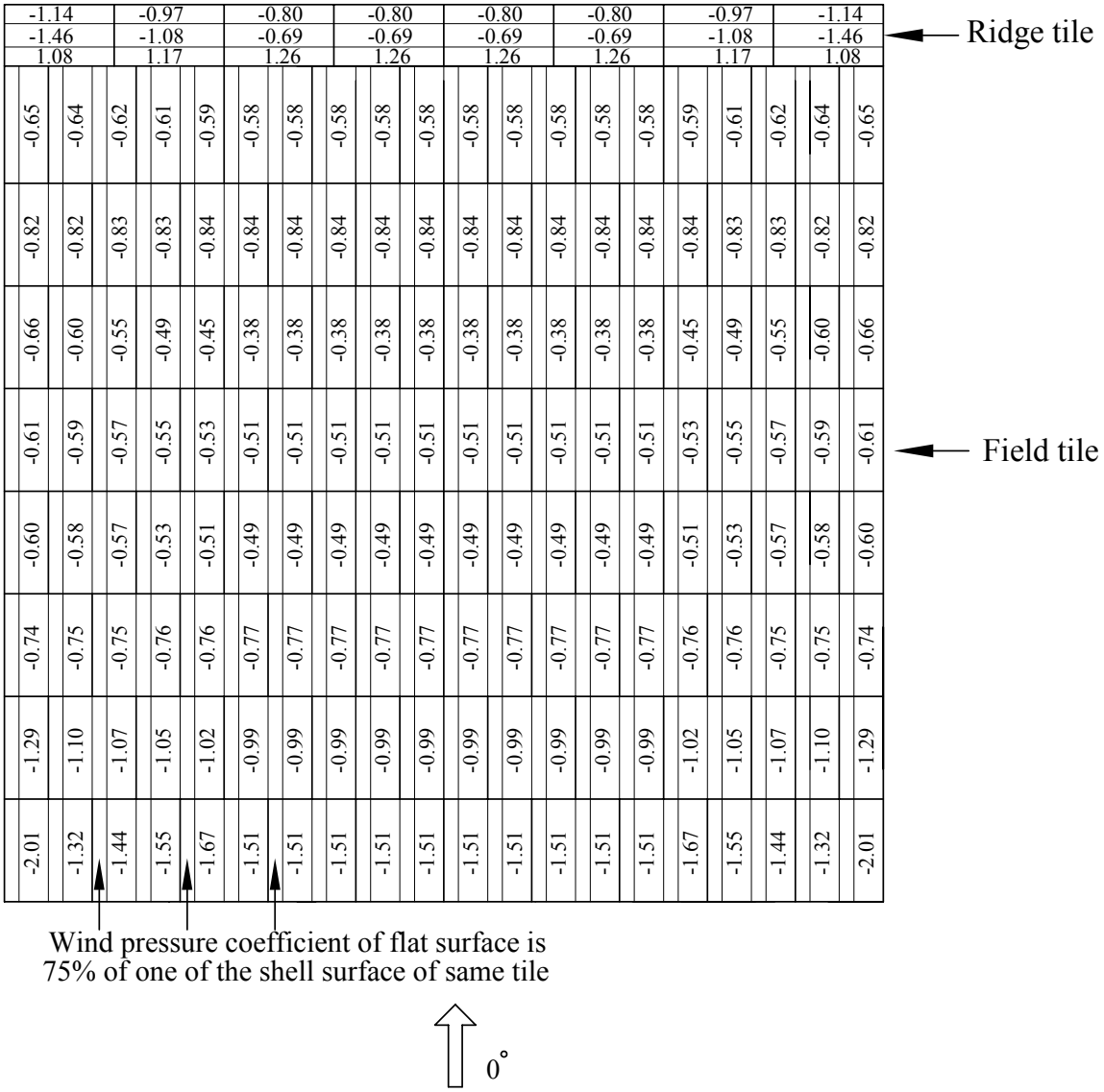

Note: The wind pressure coefficient of flat portion of concrete field tile was approximately 75% of that on the rounded surface of the tile.

Figure 6.25: Pressure Coefficients of Concrete Tile Roof with Mortar-Set Used in FEM

6.3.2 Clay Tile Roof with Adhesive-Set

The ANSYS model for the entire clay tile roof with adhesive-set (foam) is shown in Figure 6.26, which was meshed with 11,481 nodes and 12,569 elements. The roof was subjected to 120 mph wind speed in the 0° direction. Figures 6.27 and 6.28 show the contours of vertical displacements and shear stresses, respectively. The vertical displacement in the middle portion of the roof is at its largest, because of the orientation of the framing members and the supporting walls.

The failure of the tiles is mainly due to the breakage at the interface. Therefore, for a tile to remain intact, the internal forces of the equivalent springs (simulating the interface) should be within the range of their respective load-deflection curves. For the simulated roof, one ridge tile at the edge and one field tile at the corner were selected to check the integrity of the roof. The results show that at 120 mph wind speed, the largest internal force of the springs in the ridge and field tile were 11.8 lb and 71.6 lb, respectively. Comparing these values with Figures 6.9a and 6.18a indicates that the internal forces do not exceed the loading range, and therefore, the tiles should be able to withstand the applied wind pressure. However, as discussed in Section 5, a large number of tiles detached at 120 mph wind speed. This difference can be explained by the fact the interface characteristics for the FEM simulation were modeled after the mechanical uplift testing of the tiles, which included adequate adhesive (foam). The foam for those tests was placed by the manufacturer's representative, and followed the manufacturer's specifications. On the other hand, the adhesive (foam) for the Wall of Wind models was placed by the roofer, and at quite inadequate rate, as explained in Section 5. The finite element simulation therefore confirms that poor workmanship may be the primary factor in limiting the uplift resistance of residential roofs.

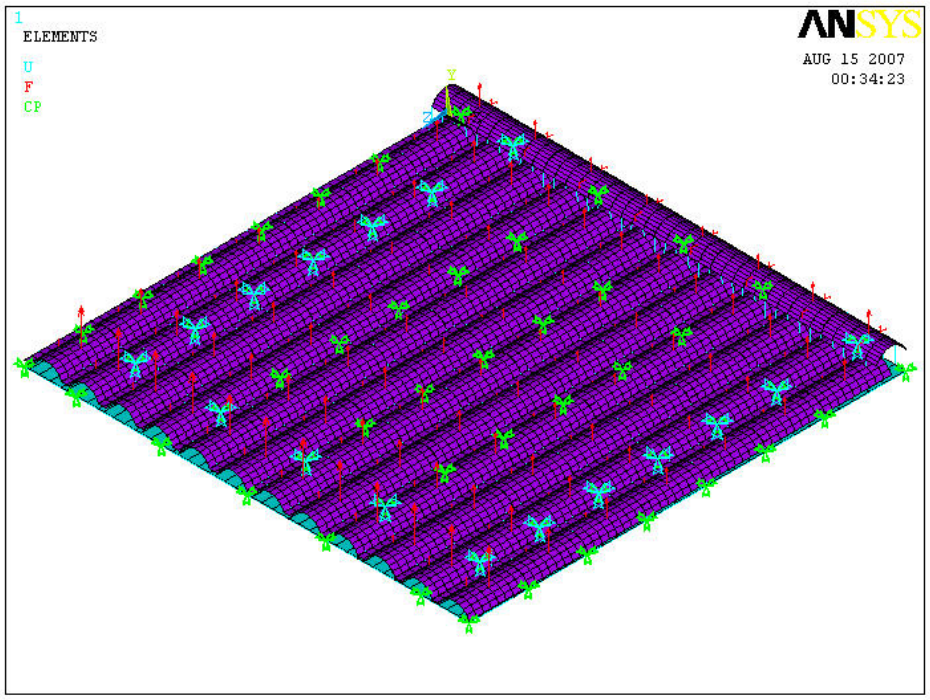

Figure 6.26: ANSYS Model of Clay Tile Roof with Adhesive-Set

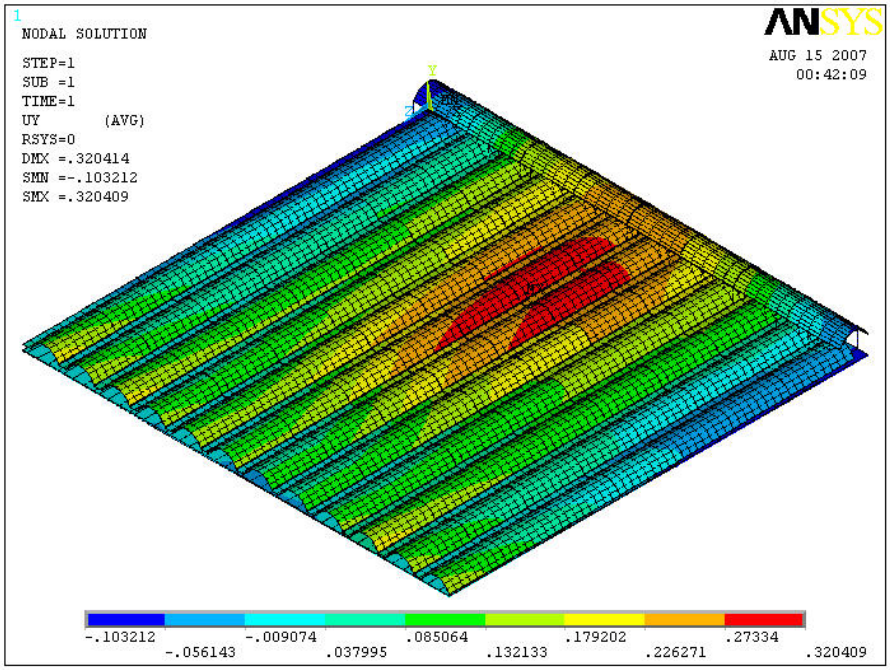

Figure 6.27: Contours of Vertical Displacements on Clay Tile Roof with Adhesive-Set for 120 mph Wind Speed at 0° Direction

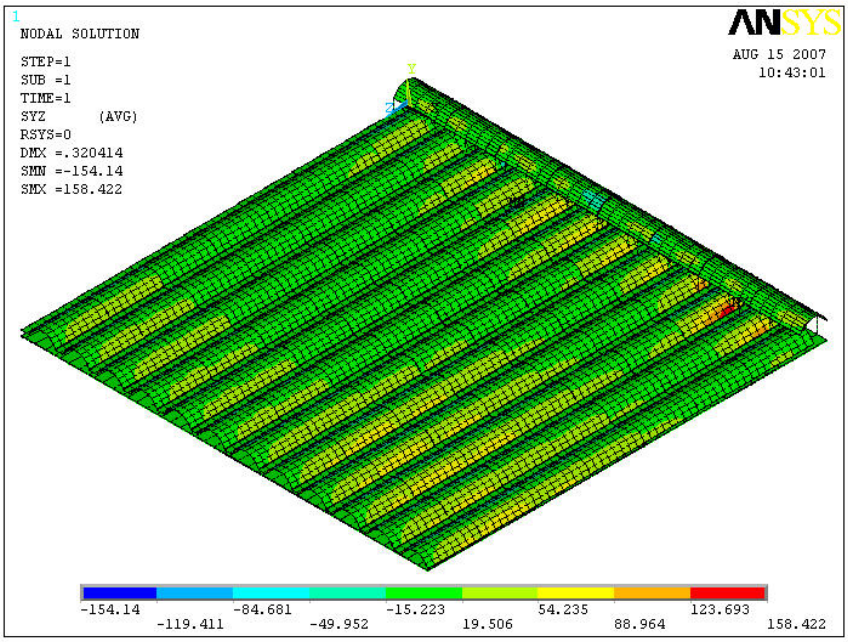

Figure 6.28: Contours of Shear Stresses on Clay Tile Roof with Adhesive-Set for 120 mph Wind Speed at 0° Direction

6.3.3 Clay Tile Roof with Mortar-Set

Figure 6.29 shows the clay tile roof with mortar-set, subjected to 120 mph wind speed at 0° direction. Figures 6.30 and 6.31 show the contours of vertical displacements and shear stresses, respectively. Similar to the adhesive-set, vertical displacement in the middle portion of the roof is at its largest, because of the orientation of the framing members and the supporting walls.

For this roof, the same two tiles as in the previous case were selected to assess whether or not the tiles would remain in place under the applied wind pressure. The results indicate that at 120 mph wind speed, the largest internal force of the springs in the two selected ridge and field tiles were 15.4 lb and 58.7 lb, respectively. Comparison of these values with Figures 6.13a and 6.21a indicate that the internal forces do not exceed the loading range, and therefore, failure of the clay tiles with mortar-set may be attributed to the poor workmanship and the inadequate amount of the mortar placed under each tile.

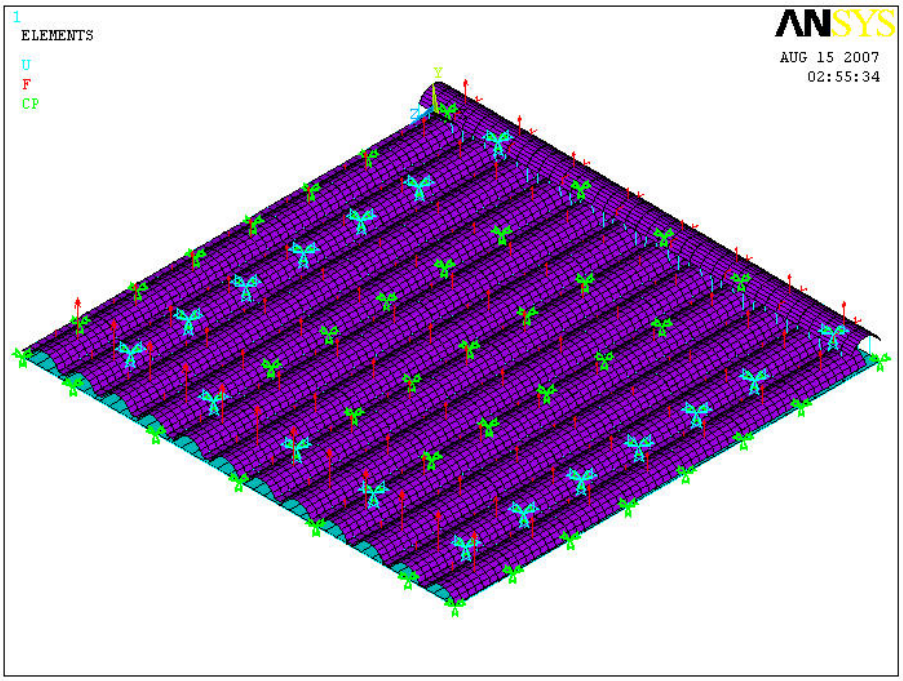

Figure 6.29: ANSYS Model of Clay Tile Roof with Mortar-Set

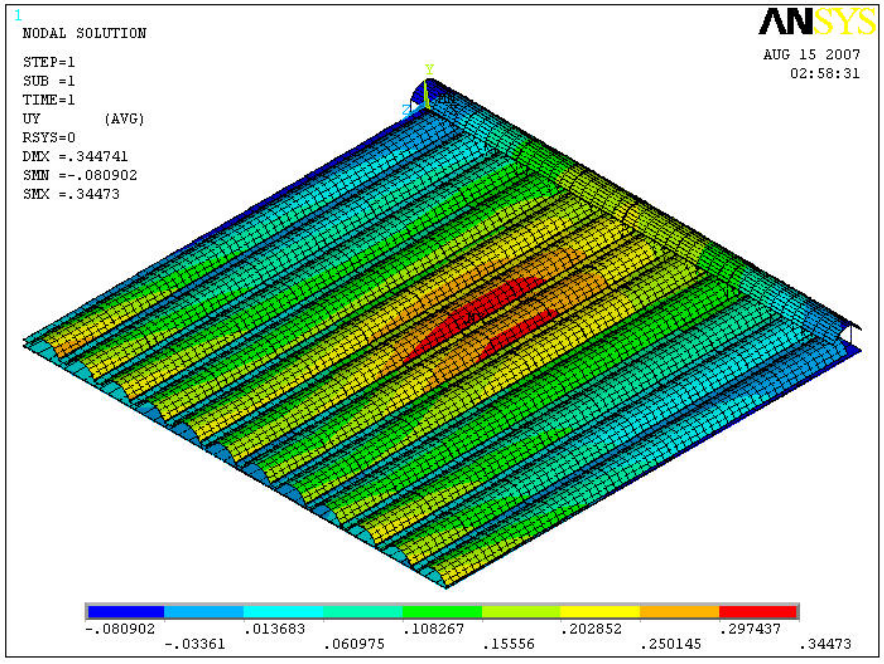

Figure 6.30: Contours of Vertical Displacements on Clay Tile Roof with Mortar-Set for 120 mph Wind Speed at 0° Direction

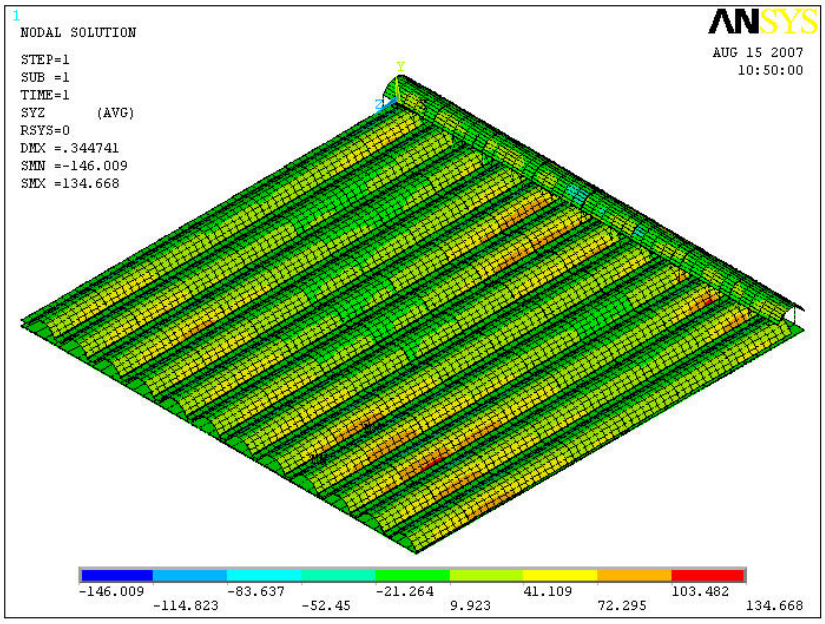

Figure 6.31: Contours of Shear Stresses on Clay Tile Roof with Mortar-Set for 120 mph Wind Speed at 0° Direction

6.3.4 Concrete Tile Roof with Adhesive-Set

The ANSYS model for the concrete tile roof with adhesive-set (foam) is shown in Figure 6.32. The finite element mesh included 13,681 nodes and 14,146 elements. The roof was subjected to 120 mph wind speed in the 0° direction. Figures 6.33 and 6.34 show the contours of vertical displacements and shear stresses, respectively. Similar to the clay tile roof, vertical displacement in the middle portion of the roof is at its largest, because of the orientation of the framing members and the supporting walls.

For this roof, the same two tiles as in the previous cases were selected to assess whether or not the tiles would remain in place under the applied wind pressure. The results indicate that at 120 mph wind speed, the largest internal force of the springs in the two selected ridge and field tiles were 13.0 lb and 36.4 lb, respectively. Comparison of these values with Figures 6.9b and 6.18b indicate that the internal forces do not exceed the loading range, and therefore, failure of concrete tiles with adhesive-set in the Wall of Wind test may be attributed to the poor workmanship and the inadequate amount of adhesive (foam) placed under each tile.

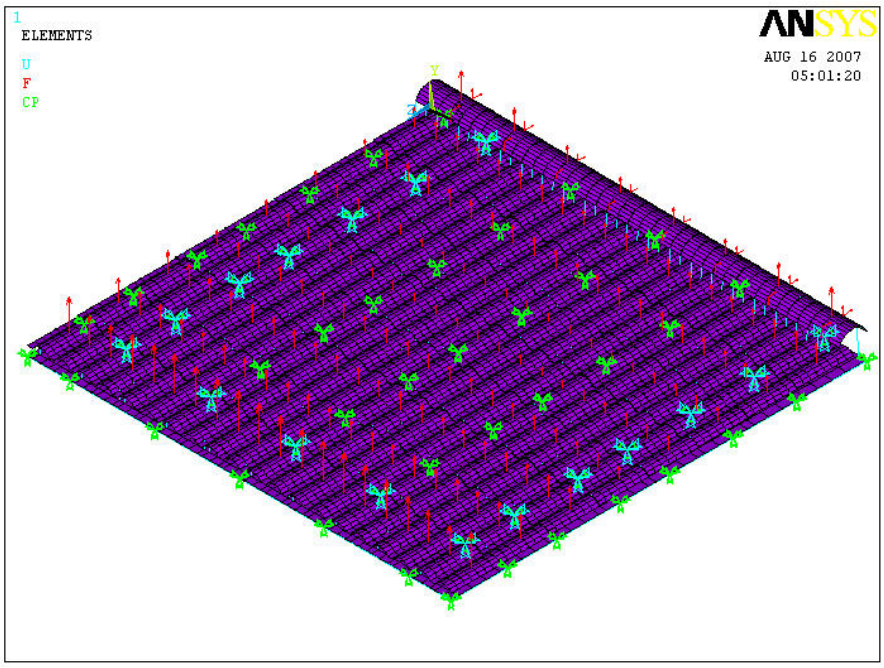

Figure 6.32: ANSYS Model of Concrete Tile Roof with Adhesive-Set

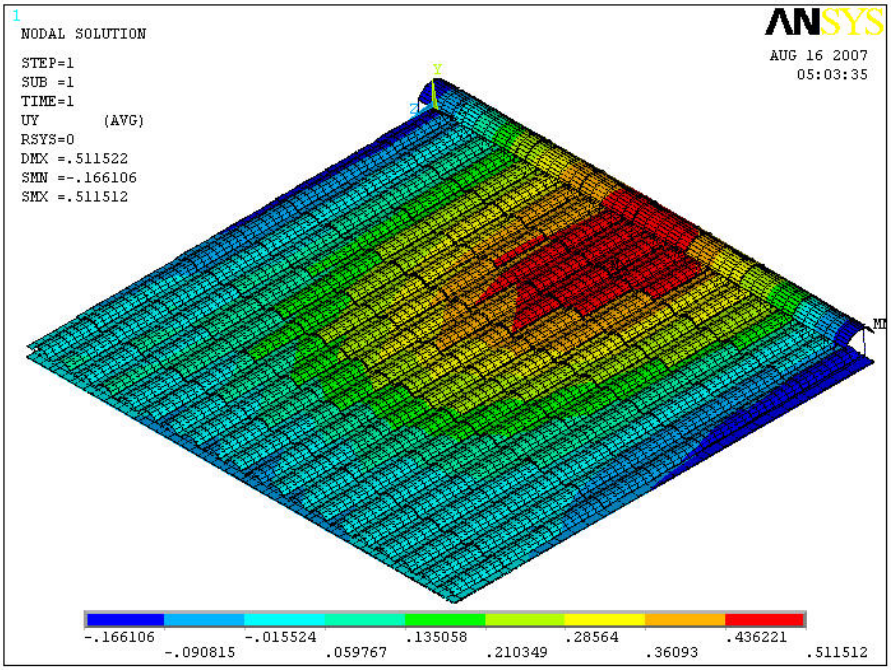

Figure 6.33: Contours of Vertical Displacements on Concrete Tile Roof with Adhesive-Set for 120 mph Wind Speed at 0° Direction

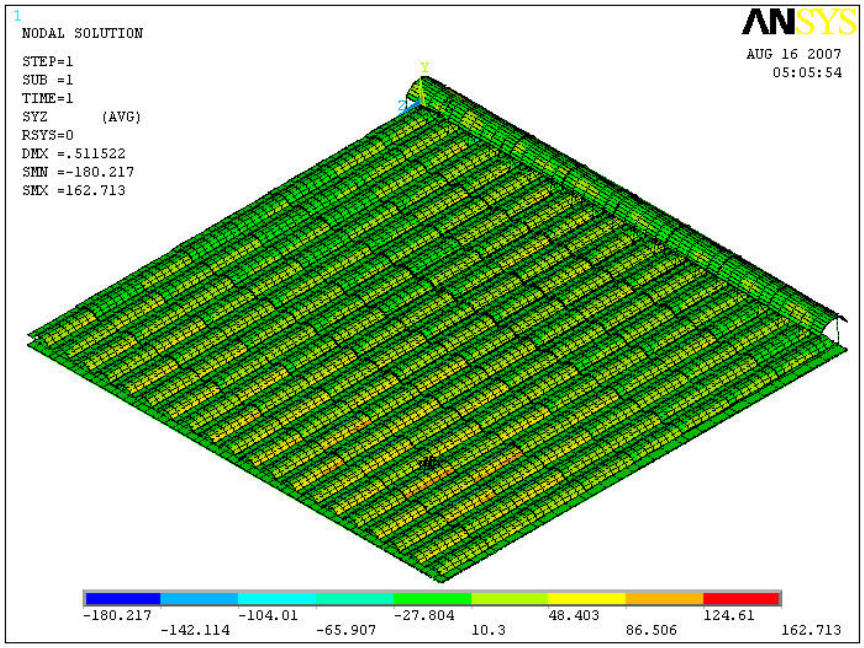

Figure 6.34: Contours of Shear Stresses on Concrete Tile Roof with Adhesive-Set for 120 mph Wind Speed at 0° Direction

6.3.5 Concrete Tile Roof with Mortar-Set

Figure 6.35 shows the concrete tile roof with mortar-set, subjected to 120 mph wind speed at 0° direction. Figures 6.36 and 6.37 show the contours of vertical displacements and shear stresses, respectively. Similar to the adhesive-set, vertical displacement in the middle portion of the roof is at its largest, because of the orientation of the framing members and the supporting walls.

For this roof, the same two tiles as in the previous case were selected to assess whether or not the tiles will remain in place under the applied wind pressure. The results indicate that at 120 mph wind speed, the largest internal force of the springs in the two selected ridge and field tiles are 16.9 lb and 41.3 lb, respectively. Comparison of these values with Figures 6.13b and 6.21b indicate that the internal forces do not exceed the loading range, and the tiles are not expected to fail.

It was noted that concrete field tiles were installed in a staggered pattern, while the clay field tiles were installed in tandem. The staggered pattern of concrete filed tiles helped form an interlocking system to resist the wind pressure. Therefore, the largest internal force of the springs in the selected concrete field tiles with adhesive-set and mortar-set are 36.4 and 41.3 lb, respectively. The corresponding values for the clay filed tiles were 71.6 and 58.7 lb, respectively. Part of this large disparity in the uplift force exerted on the tile attachment system may be attributed to the tile arrangement on the roof. The staggered arrangement of tiles seems to help distribute the uplift pressure away from the

corner and edge tiles on the roof under heavy wind loads. This is perhaps one of the reasons why concrete tile roof with mortar-set was the only model that did not fail at 120 mph wind speed in the Wall of Wind tests.

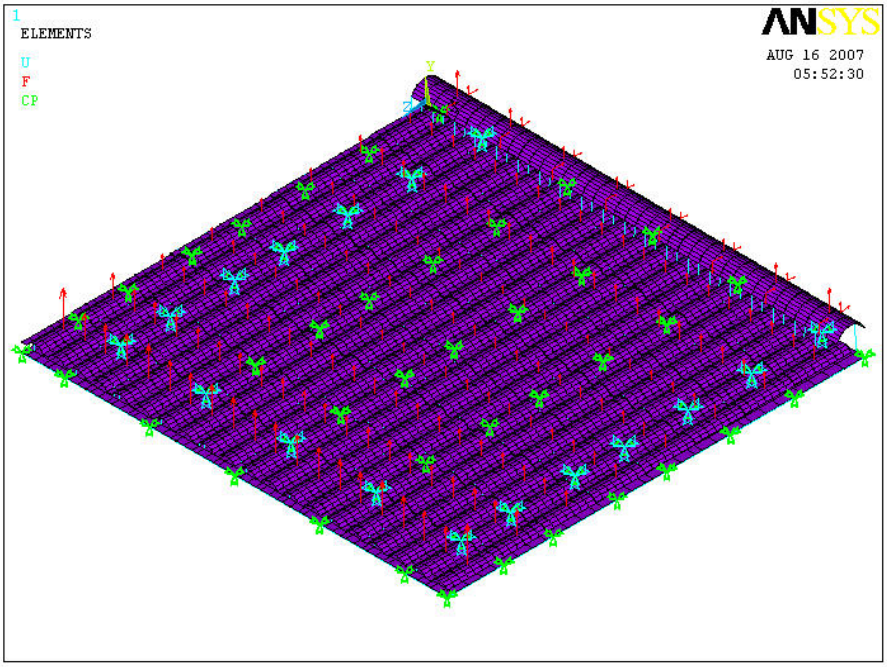

Figure 6.35: ANSYS Model of Concrete Tile Roof with Mortar-Set

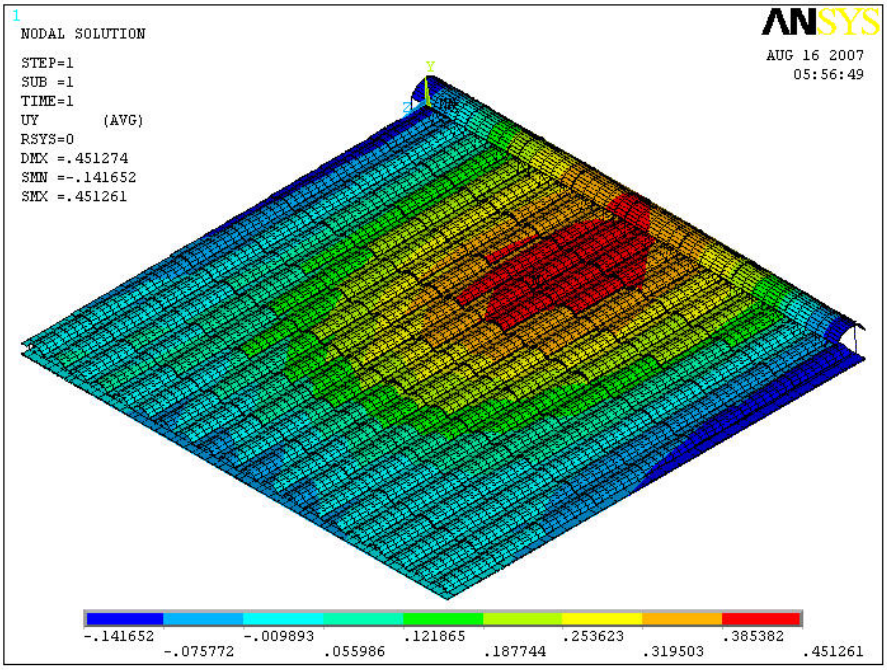

Figure 6.36: Contours of Vertical Displacements on Concrete Tile Roof with Mortar-Set for 120 mph Wind Speed at 0° Direction

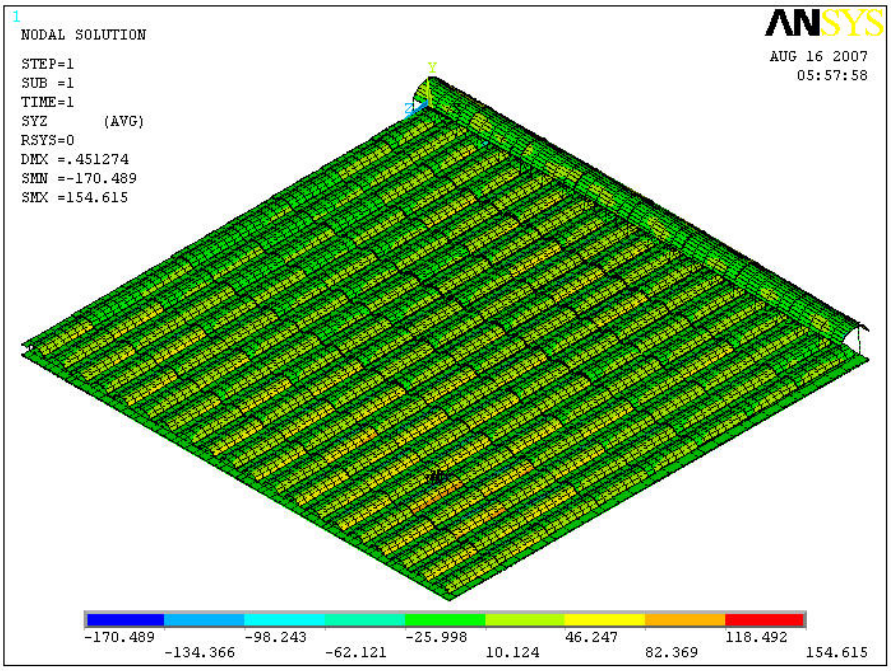

Figure 6.37: Contours of Shear Stresses on Concrete Tile Roof with Mortar-Set for 120 mph Wind Speed at 0° Direction

7.0 Conclusions

Given the extent of damages to the tile roofs incurred by Floridians in the last few years, a detailed experimental and analytical study was carried out for clay and concrete roof tiles with adhesive-set and mortar-set attachments. The study was aimed at comparing the performance of these tiles and attachment systems using: (a) monotonic and cyclic uplift tests; (b) impact tests; (c) dynamic wind simulation test using the WoW; and (d) finite element analysis. The study has resulted in the following conclusions:

- The uplift test results obtained in this phase, consistent with those of Phase 1, indicated that clay tiles perform better than concrete tiles when attached with adhesive-set, whereas concrete tiles perform much better than clay tiles when attached with mortar-set.

- Monotonic testing used by tile manufacturers across the industry tends to overestimate the uplift capacity of roof tiles by as much as 40%. Cyclic testing was found to be more accurate in evaluating the uplift performance of roof tiles. These conclusions support the recommendations of the mitigation assessment teams (MAT).

- Concrete tiles were significantly better than clay tiles in resisting projectile impact. Furthermore, they break while remaining attached to the roof when impacted by a projectile. Clay tiles were found to shatter into small pieces for the same impact energy.

- The roof system that was found to provide the highest resistance to static and dynamic uplift forces was concrete tiles attached with mortar. This conclusion was corroborated by both static and dynamic tests as well as analytical models (FEM).

- Roof tile failures were found to be initiated at the eave on the windward side of the roof. This failure was found to cause a domino failure pattern of the remaining roof tiles.

- Workmanship was found to be the main contributing factor to roof tile failures. This conclusion was confirmed by mechanical uplift tests and finite element analysis, which together showed that the roof system can resist the dynamic uplift force of the wind if built according to the code.

The above conclusions do not support recent efforts by the industry to completely ban the use of mortar for all attachments of hip and ridge tiles. The present study suggests limiting the ban of mortar-set to only clay tiles.

It is this study's recommendation that special attention be paid to the attachment of eave tiles, as they are the most vulnerable to failure. Additional attachment material should be placed between these tiles and the underlayment of the roof. This study also points out

the effect of tile setting pattern on the uplift capacity of the roof, suggesting that staggered setting of tiles would help develop an interlocking mechanism between the tiles. It is also this study's recommendation that inspection procedures be improved to ensure roofing contractors closely follow the standard techniques of roof tile installation outlined in the code.

References

_____. *(ASTM) American Standard Testing Method for* Wind Resistance of Concrete and Clay tiles, 2005.

_____. *(TAS) Testing Application Standards 101 – 95,* Test Procedure for Static Uplift Resistance of Mortar or Adhesive Systems, 1995 – 1998

_____. *Florida Building Code 2004,* Florida Department of Community Affairs, Tallahassee, FL, 2005.

_____. *Hip and Ridge Installation Instructions,* FRSA/TRI "Concrete and Clay Roof Tile Installation Manual" Fourth Edition, August 3, 2005

_____. *Hurricane Damage to Residential Structures: Risk and Management.* The Johns Hopkins University. Baltimore, Maryland, November, 1996

_____. *Hurricanes Charley and Ivan Wind Investigation Report,* Roofing Industry Committee on Weather Issues, Inc (RICOWI, Inc.), March 2006.

_____. *Mitigation Assessment Team Report, Hurricane Charley in Florida,* Observations, Recommendations, and Technical Guidance, FEMA 488 / April 2005

_____. *Mitigation Assessment Team Report, Hurricane Charley in Florida,* Observations, Recommendations, and Technical Guidance, FEMA 489 / August 2005

_____. *Report to the Florida Building Commission,* Florida State University, October 10, 2005

_____. *Summary Report Building Performance*, 2004 Hurricane Season, FEMA 490 / March 2005

American Society of Civil Engineering, ASCE 7-05 Minimum Design loads for buildings and other structures, 2005.

Analysis of proposed consent order to aid public comment; Monier Lifetime LLC-Analysis, March 1999.

C. M. Blessing, 2007. Mitigation of Roof Uplift Through Vortex Suppression Techniques, Master thesis, Department of Civil and Environmental Engineering, Florida International University.

Commission Proposes Florida Building Code Changes, Florida Homes Builders Association @ FHBA.com, May 2006.

Concrete and Clay Roof Tile Installation Guide, Fourth Edition, Florida Roofing, Sheet Metal and Air Conditioning Association, Winter Park, FL, and Tile Roofing Institute, Chicago, 2005.

FHBA/HBAMO Water Intrusion Study Recommendations; Florida Homes Builders Association @ FHBA.com, May 2006.

Florida Building Commission Approves Unified Building Code; Flsenate.gov; November 2000.

From the Florida Building Code Preface History; 2004 Florida Building Code Volume p/5601104; April 2006.

Hurricane Research Advisory Committee, Report to The Florida Building Commission,
International Building Code, International Code Council Inc., Falls Church, VA, 2003.

Metal Building Systems Manual; Metal Building Manufacturers Association, Cleveland, OH, 2002.

Minimum Design Loads for Buildings and Other Structures, ASCE-7 2002, Structural Engineering Institute of the American Society of Civil Engineers, Reston, VA.
Mitigation Assessment Report: Hurricane Andrew Florida; FEMA FIA-22, June 2005.

NOAA Issues 2005 Atlantic Hurricane Season outlook; NOAA News @ noaa.gov, May, 2005.

Roof Damage Issues in Hurricanes; Haag Engineering Company, Timothy P Marshall, P.E.; 2455 S McIver Dr., Carrollton TX 75006. October 10, 2005

Roof tiles Scarce, Soaring in price. Palm Beach Post, April 2006.

Tile Roof Assn. issues new guidelines after Hurricane findings; buildingonline.com/news/ October 2005.

Tile Roofing for High-Wind Areas; FEMA 499, Technical Fact Sheet No. 21, August 2005.

Tile Roofing Institute Surveys Hurricane Charley Damage; Industry Association Aids in Damage Assessment and Provides Advice to Homeowner; Business Wire, August, 2004